THE GEOLOGICAL SOCIETY OF AMERICA®

Paleoelevation variations and exhumation history of the Tibetan Plateau control spatiotemporal distribution of porphyry system deposits

Peng Zhang[1,2], Zhenjie Zhang[1,†], Mark J. Hoggard[2], and Qiuming Cheng[1,3]

[1]*School of Earth Sciences and Resources, Frontiers Science Center for Deep-time Digital Earth, State Key Lab of Geological Processes and Mineral Resources, China University of Geosciences, Beijing 100083, China*

[2]*Research School of Earth Sciences, Australian National University, Canberra 2601, Australia*

[3]*School of Earth Science and Engineering, Sun Yat-sen University, Zhuhai 519082, China*

ABSTRACT

Porphyry deposits, due to their significant size and economic value, have long been a focus of research. Nevertheless, the majority of studies concentrate on the genesis of porphyry deposits, with relatively few considering how post-formation preservation conditions go on to influence their present-day distribution. The unique geographical setting of the Tibetan Plateau makes it a key region for investigating the interplay between ore deposits, tectonic deformation, and geomorphic evolution in an intraplate setting. In particular, its abundant tectonic and magmatic events have facilitated the formation of numerous porphyry deposits. This study combines big datasets of whole-rock geochemistry, zircon geochronology, and low-temperature thermochronology to reconstruct the tectonic and magmatic evolution, paleoelevation variations, and exhumation history of various terranes within the Tibetan Plateau since Jurassic times and explores how these processes relate to the formation and preservation of porphyry deposits. Our results show that the Qiangtang terrane contains a higher and more clustered concentration of porphyry Cu-Au deposits during intervals of decreasing paleoelevation, whereas the Lhasa terrane predominantly hosts porphyry Cu-(Mo) deposits during intervals of increasing paleoelevation. We propose that intense tectonic and magmatic activity is a critical factor in the formation of porphyry deposits, while significant fluctuations in the paleoelevation of terranes also favor their development. Conversely, regions of the Tibetan Plateau with high degrees of exhumation host fewer porphyry system deposits, and their deposits tend to be of smaller tonnage. This indicates that post-formation exhumation plays a critical role in the preservation of porphyry deposits, with intense exhumation likely leading to erosional loss of previously formed deposits. Areas with lower exhumation volumes should therefore be prioritized as key targets for future mineral exploration.

1. INTRODUCTION

Porphyry systems are notable for their large mineralization volumes, shallow burial depths, and uniform ore grades, making them one of the principal global sources of metals such as copper (Cu), molybdenum (Mo), and gold (Au; Richards, 2003, 2015; Sillitoe, 2010). The classic porphyry system model established by Sillitoe (2010) includes porphyry deposits located in the deeper central part of the complex, Cu, Au, and/or zinc (Zn) skarns formed in contact zones with carbonate strata, and epithermal orebodies located in shallower strata overlying the main porphyry body (Sillitoe, 2010; Mao et al., 2014; Richards, 2015). Porphyry system deposits (PSDs) typically form within oceanic or continental arcs above subduction zones on active continental margins (Sillitoe, 1972; Richards, 2003; Wilkinson, 2013). However, recent studies have demonstrated that continental collision orogenic belts also represent important settings for the formation of PSDs (Richards, 2009; Hou et al., 2015; Yang and Cao, 2024). These environments facilitate low-angle underthrusting and subduction, crustal shortening and thickening, uplift, erosion, and contemporaneous adakitic magmatism that are all thought to contribute to the formation of PSDs (Cooke et al., 2005). Due to the fact that most PSDs form at shallow depths (typically 1–6 km, with a consistent average of ~2 km; Wilkinson and Kesler, 2007; Yanites and Kesler, 2015), prolonged tectonic activity and exhumation processes may result in the uplift and exposure of older PSDs to the surface, leading to their degradation (Wilkinson and Kesler, 2007; Leng et al., 2018). As a consequence of this survivor bias, known porphyry deposits around the world typically have Phanerozoic ages, with a majority concentrated in the Cenozoic Era (Singer et al., 2008). Therefore, knowing the tectonic evolution and exhumation processes following PSD mineralization is crucial for assessment of mineral resource potential and exploration (Wilkinson and Kesler, 2007; Gong et al., 2021).

The Tibetan Plateau has a rich history of magmatic activity and tectonic evolution, making it one of the most important regions for PSDs. It has undergone multiple phases of tectonic uplift and prolonged exhumation. Regional differences in the timing and pattern of uplift have resulted in differential exposure across the Tibetan Plateau, which has consequences for the preservation potential of deep-seated mineral deposits across the orogen (Kesler and Wilkinson, 2006; Bierlein et al., 2016; Min and Gao, 2022; Leng et al., 2018). Nevertheless, the timing, duration, and rates of differential uplift of the Tibetan Plateau remain a subject of much debate, with many valuable contributions over the past two decades. Techniques including clumped isotopes (Rowley and Currie, 2006; Ding et al., 2014; Ingalls et al., 2018; Xiong et al., 2020; Xu et al., 2022), fossil assemblages (Spicer et al., 2003; Hu et al., 2016b; Ding et al., 2017; Su et al., 2019a; Zhang et al., 2022), whole-rock geochemistry on magmatic rocks (Zhu et al., 2017; Hu et al., 2020), and others have been used to infer paleoelevation histories across the plateau; however, these studies have yielded inconsistent results. Moreover, previous research has primarily focused on the paleoelevation variation processes of the Tibetan Plateau without establishing a connection to the mineralization and preservation of porphyry deposits. The evolution pattern of pla-

Zhenjie Zhang https://orcid.org/0000-0003-1079-8784

†zjzhang@cugb.edu.cn

GSA Bulletin;
Published online 4 March 2026

https://doi.org/10.1130/B38560.1.

teau paleoelevation and its relationship with porphyry systems remain to be further investigated.

Apatite and zircon (U-Th)/He dating and fission-track thermochronological methods, due to their relatively low closure temperatures, are capable of recording thermal regimes occurring within the topmost few kilometers of the upper crust. These methods are widely applied to studies of Cenozoic mountain uplift and tectonic evolution (Farley and Stockli, 2002; Kirby et al., 2002; Clark et al., 2005; Ouimet et al., 2010; Wilkinson, 2013; Tian et al., 2014; Zhang et al., 2015; Wang et al., 2016; Tan et al., 2017; Cao et al., 2022; Zhao et al., 2022a; Yin et al., 2023; Zhang et al., 2024a). A suite of recent studies have harnessed apatite and zircon thermochronology to constrain the cooling and exhumation histories of porphyry deposits in the Tibetan Plateau, and corresponding datasets have been established for specific areas of interest (e.g., Ouimet et al., 2010; Wilson and Fowler, 2011; Li et al., 2014; Tian et al., 2014; Zhang et al., 2015; Wang et al., 2016; Zhao et al., 2016; Tan et al., 2017; Leng et al., 2018; Yang et al., 2020; Cao et al., 2022; Su et al., 2022; Yang et al., 2022a, 2022b; He et al., 2023; Zhang et al., 2024a, 2024b). These studies not only quantify the thermal histories of deposits and determine their uplift and exhumation rates, but also provide a reliable technical foundation for exploring the influence of regional tectonic evolution on deposit preservation potential. Nevertheless, previous research has primarily focused on specific mining districts or localized regions, with a lack of comprehensive studies addressing the entire Tibetan Plateau. The impact of post-mineralization exhumation on the spatiotemporal distribution of PSDs in the Tibetan Plateau remains poorly constrained. Therefore, compiling, integrating, and analyzing the existing disparate thermochronological data from across the Tibetan Plateau to reconstruct its spatiotemporal exhumation history is likely to be of great value in furthering our understanding of the regional tectonic evolution in relation to its porphyry deposits endowment.

In this study, we begin by compiling a series of datasets from across the Tibetan Plateau, including the location and formation ages of PSDs, the geochemistry of igneous rocks (both whole-rock and zircon geochemistry), and thermochronological data including (U-Th)/He and fission-track analyses of zircon and apatite minerals. We then reconstruct the regional paleoelevation and exhumation history and compare it to the spatiotemporal distribution of porphyry deposits. This study aims to synthesize constraints on the tectonic events, growth, and evolution of the Tibetan Plateau, offering new evidence to address existing controversies in the field, while also investigating the influence of tectonic-magmatic activities on PSD mineralization and subsequent preservation, thereby providing novel insights for enhanced exploration targeting.

2. GEOLOGICAL SETTING

The Tibetan Plateau is the highest and most extensive topographic feature on Earth, covering an area ~3500 × 1500 km and including 82% of the world's surface area that resides >4 km above sea level (Fielding et al., 1994; Fig. 1). Its complex and rapid evolution has created a diverse geological and topographic landscape that has long been regarded as a key area for exploring mechanisms of intraplate deformation and interactions between active tectonics, landscape evolution, and paleoclimate (An et al., 2001; Clark et al., 2005; Dupont-Nivet et al., 2007). Over the past ~300 m.y., several terranes have collided due to the subduction of intervening oceanic basins during closure of the Tethys Ocean (Allégre et al., 1984; Yin and Harrison, 2000; Ding et al., 2022). From north to south, the principal suture zones of the Tibetan Plateau include the Ayimaqin-Kunlun suture zone, Jinsha suture zone, Bangong-Nujiang suture zone, and Yarlung-Tsangpo suture zone. These suture zones divide the plateau into five major accretionary terranes from north to south: the Kunlun-Qaidam, Hoh Xil–Songpan Garze, Qiangtang, Lhasa, and Himalayan terranes (Fig. 1). Addi-

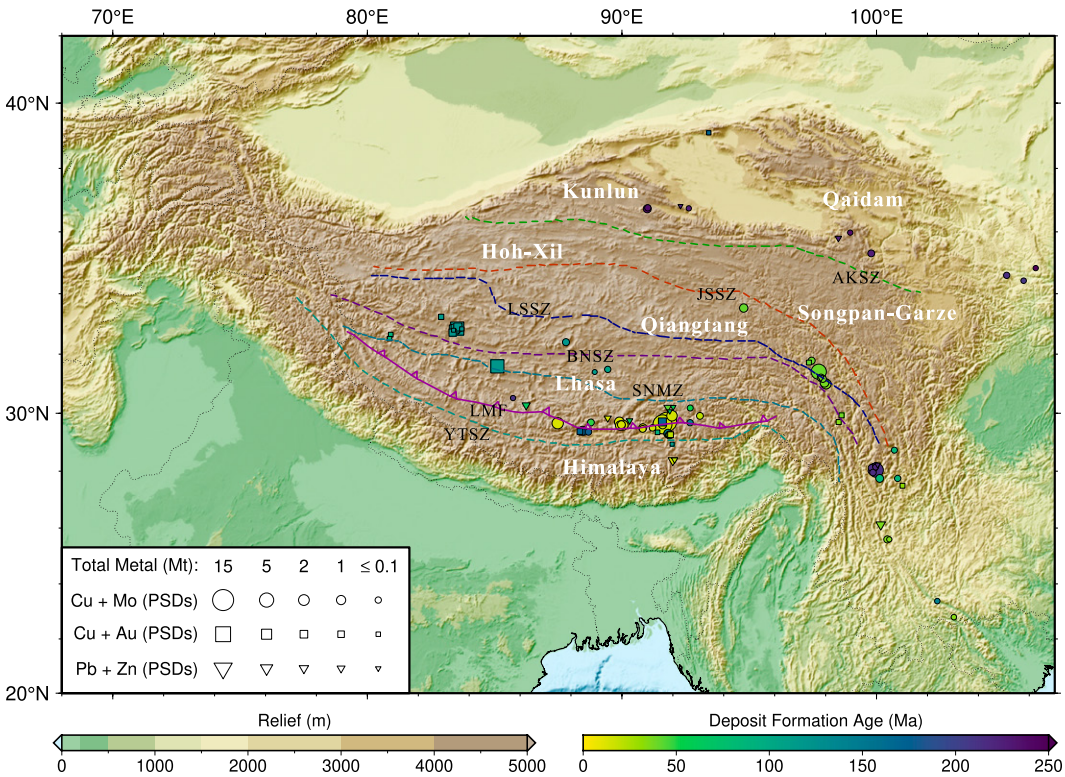

Figure 1. Topography, major crustal terranes, and porphyry deposits of the Tibetan Plateau. Symbols represent different sub-types of porphyry system deposits (PSDs), scaled by total metal content and colored by formation age. AKSZ—Ayimaqin-Kunlun suture zone; JSSZ—Jinsha suture zone; BNSZ—Bangong-Nujiang suture zone; YTSZ—Yarlung-Tsangpo suture zone; LSSZ—Longmu Co–Shuanghu suture zone; LMF—Luobadui-Milashan fault; SNMZ—Shiquanhe-Nam Tso mélange zone. Suture zone data from Yin and Harrison (2000).

tionally, the Longmu Co–Shuanghu suture zone separates the Qiangtang terrane into the North Qiangtang and South Qiangtang sub-terranes. The Lhasa terrane is further divided into northern, central, and southern Lhasa sub-terranes, bounded by the Luobadui-Milashan fault and the Shiquanhe–Nam Tso mélange zone. These multiple subduction and collision events have led to the formation of a highly heterogeneous lithosphere in the plateau region, as well as a complex history of crustal deformation and surface elevation changes (Ding et al., 2022).

Ideas concerning the growth history of the Tibetan Plateau have evolved from synchronous, essentially uniform uplift to punctuated periods of episodic and spatially localized growth (Molnar et al., 1993; Mulch and Chamberlain, 2006; Wang et al., 2008b; Ibarra et al., 2023). Recent decades have seen the development of concepts including the northward growth model (Tapponnier et al., 1982, 2001; Mulch and Chamberlain, 2006), the eastward expansion model (Royden et al., 1997, 2008; Clark and Royden, 2000; Cao et al., 2022), the proto-Tibetan Plateau model (Kapp et al., 2007; Wang et al., 2008a, 2008b; Rohrmann et al., 2012; Wang et al., 2014; Ibarra et al., 2023), and the central Tibetan valley model (Rowley and Currie, 2006; Ding et al., 2014; Su et al., 2019b, 2020; Spicer et al., 2021; Ibarra et al., 2023). Although perspectives vary, most previous studies agree that the majority of the present-day relief developed primarily due to collision between the Indian and Eurasian continents from 65 Ma to 45 Ma (Molnar et al., 1993; Mulch and Chamberlain, 2006; Zhu et al., 2015; Hu et al., 2016a; Ibarra et al., 2023).

The Tibetan Plateau exhibits intense tectonic activity, preserving a detailed record of processes ranging from subduction of Tethyan oceanic crust through to collision of the Indian and Asian continental plates (Tang, 2019). Magmatic rocks and porphyry metallogenesis span the entire period from oceanic subduction to continental collision (Fig. 1). These deposits are primarily concentrated within three distinct metallogenic belts: (1) the Gangdese belt of the southern Lhasa terrane, with primary diagenetic and metallogenic ages concentrated in Early to Middle Jurassic, Paleocene, Oligocene, and Miocene times; (2) the Bangong-Nujiang belt; and (3) the Yulong belt, which respectively straddle the western and eastern sections of the boundary between the Lhasa and Qiantang terranes and have deposits predominantly with Early Cretaceous to Eocene formation ages.

Subduction-related porphyry copper deposits are associated with calc-alkaline arc magmas, which derive from a metasomatized asthenospheric mantle wedge (Richards, 2003; Sillitoe, 2010). These deposits are predominantly characterized by copper mineralization, often accompanied by gold and silver (Ag), as exemplified by the Xiongcun, Tiegelongnan, Duobuza, and Bolong deposits. In contrast, collision-related porphyry copper deposits are linked to mildly alkaline magmas, which form by remelting of arc lithosphere that has previously been modified by subduction (Richards, 2009; Hou et al., 2023). A subset are often associated with crustal thickening and include a series of skarn-type lead (Pb)-Zn(-Cu-Au-Ag) deposits, such as Mengya'a and Dongzhongla, as well as low-sulfidation, epithermal Ag-Pb-Zn(-Au) deposits. Deposits associated with strike-slip faulting include porphyry-skarn Cu-Mo-tungsten deposits such as Yulong and Nuri-Chengba. Meanwhile, deposits formed in an extensional setting include porphyry-skarn Cu-polymetallic deposits such as Qulong, Jiama, Bangpu, and Zhuno (Tang et al., 2024).

3. DATA AND METHODS

3.1. Tibetan Plateau Mineral Deposits

In this study, we compiled information data on PSDs (including porphyry, skarn, and epithermal deposits) within the age range of 250 Ma on the Tibetan Plateau (Fig. 1). Specifically, there are 22 porphyry system Cu-Au deposits, 14 porphyry system Pb-Zn deposits, and 55 porphyry system Cu(-Mo) deposits. Furthermore, we categorized the tonnage of the deposits into five levels: $<$ 0.1 Mt, 0.1–1 Mt, 1–2 Mt, 2–5 Mt, and 5–15 Mt. Detailed information on the deposits is presented in Table S1 in the Supplemental Material.[1]

3.2. Whole-Rock Geochemistry

The whole-rock geochemical data used in the study were sourced from the Tibetan Plateau magmatic rock dataset (Chapman and Kapp, 2017), EarthChem (https://earthchem.org/), and GEOROC (https://georoc.eu/georoc/new-start.asp) databases. Each data point includes 10 major elements (SiO_2, TiO_2, Al_2O_3, FeOT, MnO, MgO, CaO, Na_2O, K_2O, P_2O_5) and 22 trace elements (La, Ce, Pr, Nd, Sm, Eu, Gd, Tb, Dy, Ho, Er, Tm, Yb, Lu, Sr, Y, Rb, Ba, Hf, Nb, Ta, Th). The collected dataset of whole-rock magmatic rocks was utilized to reconstruct paleoelevation changes on the Tibetan Plateau, and thus, each data point also required age and coordinates. To eliminate mafic samples and extreme outliers, only data with SiO_2 content between 55 wt% and 75 wt% and MgO $\leq$ 6 wt% were included (Guo and Yang, 2023).

After screening, the data on magmatic rocks from the Himalayan and Kunlun-Qaidam terranes were found to be insufficient to reconstruct paleoelevation changes. Therefore, this study focuses on the paleoelevation changes of the Lhasa and Qiangtang terranes. A total of 2701 magmatic rock data points with ages spanning 200 m.y. were collected from these two terranes, including 773 data points from South Lhasa, 1027 from Central and North Lhasa, and 901 from Qiangtang terrane. Detailed data can be found in Table S2. The spatiotemporal distribution of the data is presented in Figure S1.

3.3. Paleoelevation Records

Previous studies have quantitatively reconstructed paleoelevations of the Tibetan Plateau during different periods and at various locations using stable isotopes of water, carbonate clumped isotope thermometry, coexistence approach of organisms, and other methods. These reconstructions have provided crucial constraints on the timing and geodynamic mechanisms of continental deformation and plateau growth. To compare with the results of this study, we compiled published paleoelevation data from the literature, encompassing $\sim$136 paleoelevation records from different terranes of the Tibetan Plateau (Table S3). However, existing paleoelevation data for the Tibetan Plateau are predominantly focused on the Cenozoic, with scarce studies on paleoelevation reconstruction before the collision between the Indian and Eurasian continents. Furthermore, differences in reconstruction methods may lead to varying results, potentially resulting in significant discrepancies between certain outcomes.

3.4. Thermochronology

Low-temperature thermochronology data can quantitatively constrain the history of surface cooling by reconstructing the spatiotemporal patterns of erosion and tectonic exhumation, inferring the timing and magnitude of topographic variations (Reiners and Brandon, 2006; Reiners, 2007). In this study, a total of 5460 low-temperature thermochronological data points were collected from the Tibetan Plateau region, including 1012 apatite (U-Th)/He ages, 2770 apatite fission-track ages, 887 zircon (U-Th)/He ages, and 791 zircon fission-track ages (Table S4).

3.5. Zircon U-Pb Age

The zircon U-Pb age data points used in this study for investigating magmatic activity peri-

[1]Supplemental Material. Tables S1–S7 and Figure S1. Please visit https://doi.org/10.1130/GSAB.S.31378654 to access the supplemental material; contact editing@geosociety.org with any questions.

ods on the Tibetan Plateau were sourced from the GEOROC database and magmatic rock dataset (Chapman and Kapp, 2017). Each data point includes coordinate information to ensure it can be assigned to specific terranes, thereby reflecting the magmatic activity characteristics of different terranes. Since all ages discussed in this study are under 200 Ma, the $^{206}Pb/^{238}U$ ratio was interpreted as the zircon crystallization time (Black et al., 2003). Meanwhile, Data points with Th/U <0.1 were excluded to eliminate the influence of metamorphic zircons (Cavosie et al., 2004). Additionally, to ensure the quality of the data samples, only magmatic zircon grains with concordant ages were retained, i.e., 90% < age($^{207}Pb/^{235}U$)/age($^{206}Pb/^{238}Pb$) < 110% (Zhang et al., 2023). Finally, ~20,000 records were retained in the dataset for magmatic zircons in the Tibetan Plateau. The detailed data are available in Table S5.

3.6. Paleoelevation Calculation

This study utilized the whole-rock dataset to calculate the paleoelevation of the Tibetan Plateau through a two-step process. The first step involved modeling the historical variations in crustal thickness of different terranes of the plateau using the quantitative model for continental crustal thickness (Guo and Yang, 2023). This model was developed based on magmatic rock data from the GEOROC database and constructed using the extremely randomized tree machine learning method. The elemental types in the model's training set were consistent with the whole-rock geochemical data used in this study, and the corresponding crustal thickness values for the training dataset were derived from the CRUST1.0 model (Laske et al., 2013). The second step applied the crustal thickness to paleoelevation conversion method (Zhu et al., 2017) to calculate the paleoaltitudinal variations in different regions. The conversion formula is paleoelevation = (calculated crustal thickness − normal crustal thickness)/[crustal density/(lithospheric mantle density − crustal density)], where normal crustal thickness is 37 km, average crustal density is 2.77 g/cm^3, and lithospheric mantle density is 3.27 g/cm^3 (He et al., 2014; Zhu et al., 2017).

3.7. Exhumation Rate Calculation

With the thermochronology dataset, we employ a one-dimensional thermal model assuming vertical exhumation and thermal steady-state to estimate exhumation rates of the Tibetan plateau. This model takes into account parameters such as sea-level temperature, atmospheric lapse rate, geothermal gradient, thermal diffusivity, and model thickness and is applicable to different thermochronometric systems (see van der Beek and Schildgen, 2023, for details). We utilize thermochronological data from the past 30 m.y. to investigate variations in exhumation across different regions of the Tibetan Plateau. The 30 m.y. is divided into two time intervals: 30–15 Ma and after 15 Ma. For each interval, exhumation rates are calculated based on the thermochronological data, enabling the application of appropriate model parameters for each time period. The parameters used in the article are shown in Table S6.

4. RESULTS AND DISCUSSION

4.1. Tectonic and Magmatic Activity of the Tibetan Plateau

Since the four thermochronological systems (zircon fission-track, zircon (U-Th)/He, apatite fission-track, and apatite (U-Th)/He) employed in this study cover a closure temperature range of ~260 °C to 60 °C, these systems exhibit a high sensitivity to changes in upper crustal temperatures induced by tectonic or geomorphic processes. This sensitivity enables the reconstruction of long-term exhumation histories and imposes constraints on landscape evolution over large spatial scales (e.g., Reiners, 2007; Rohrmann et al., 2012; Cao et al., 2022; Zhang et al., 2024a, 2024b). Figure 2 displays the kernel density curves of the low-temperature thermochronology datasets and frequency histograms of the magmatic zircon age dataset, which can effectively reflect the intensity of tectonic and magmatic activity in different terranes of the Tibetan Plateau over a time span of 200 m.y. The Kunlun-Qaidam terrane lacks zircon (U-Th)/He analysis data, showcasing only the kernel density curves of the other three thermochronological systems data.

The Kunlun-Qaidam terrane experienced significant tectonic activity during the Late Triassic (Fig. 2A). This activity was driven by the intense subduction of the Paleo-Tethys Ocean plate as a result of the Indosinian orogeny. The northward subduction of the Tethys Ocean plate exerted compressional forces on the northern Kunlun-Qaidam terrane, leading to pronounced crustal shortening and thickening in the Late Triassic (Hu et al., 1999; Xia et al., 2014a; Liu et al., 2020). The effects of Paleo-Tethys subduction persisted into the Early Jurassic and served as a key mechanical mechanism controlling the development of a series of Jurassic foreland basins in the Qaidam region (Hu et al., 1999). During the Early Cretaceous, the initial uplift and erosion of the Qilian Mountains occurred ca. 120 Ma, influenced by the collision between the Lhasa terrane and the Eurasian continent (Vincent and Allen, 1999; Jolivet et al., 2001). Simultaneously, the southward subduction of the Eurasian continent and terrane accretion altered the regional extensional regime in the West Qinling region (Ratschbacher et al., 2003; Craddock et al., 2012). Upwelling of asthenospheric material in this extensional environment triggered regional magmatic activities (Li et al., 2013). Following the ca. 65 Ma India-Eurasia collision, tectonic activity became widespread across the northern plateau (Li et al., 2015; Qi et al., 2016). It is now widely accepted that the collision first affected the northern plateau during the Oligocene, leading to crustal shortening and thickening (e.g., Kapp and DeCelles, 2019; Ding et al., 2022; Liu et al., 2025). Although the results of this study cannot directly determine when the continental collision began to influence the Kunlun-Qaidam terrane, they indicate that tectonic activity in the terrane reached its peak intensity ca. 25 Ma (Fig. 2A). This is consistent with the hypothesis that ca. 30 Ma, the Asian lithosphere (Qaidam terrane) underwent southward subduction beneath the Hoh Xil Basin into the mantle to significant depths (Tapponnier et al., 2001; Ding et al., 2003; Ye et al., 2015; Qi et al., 2020).

The Hoh Xil–Songpan Garze terrane has experienced intense tectonic activity since 50 Ma (Fig. 2B). During the Eocene–Oligocene, the southward subduction of the Asian continental lithosphere caused crustal shortening in the Hoh Xil Basin between 51 Ma and 27 Ma, leading to the formation of a thickened lithospheric mantle (Staisch et al., 2014, 2016; McRivette et al., 2019). With the continued northward subduction of the Indian continent and the southward subduction of the Asian continent, delamination and faulting occurred in both continents ca. 25 Ma (Qi et al., 2020; Ding et al., 2022). The resultant asthenospheric upwelling triggered magmatism in the Hoh Xil Basin during this period (Turner et al., 1996) and simultaneously led to the rapid surface uplift of the Himalayan terrane, the Hoh Xil region, and the Kunlun Mountains (Qi et al., 2020). This also explains the concentration of widespread magmatic activity in the Hoh Xil Basin within ~25 m.y. (Fig. 2B). In contrast, the eastern Songpan-Garze terrane experienced a relatively stable history during the Jurassic and Cretaceous, with no major tectonic events occurring between 150 Ma and 30 Ma (Xu and Kamp, 2000; Reid et al., 2007; Roger et al., 2010). Most post-orogenic exhumation in this region occurred after 30 Ma in response to the India-Asia continental collision (Xu and Kamp, 2000; Jolivet et al., 2001; Roger et al., 2010; Wilson et al., 2006). The Tertiary deformation of the Songpan-Garze terrane can be viewed, to some

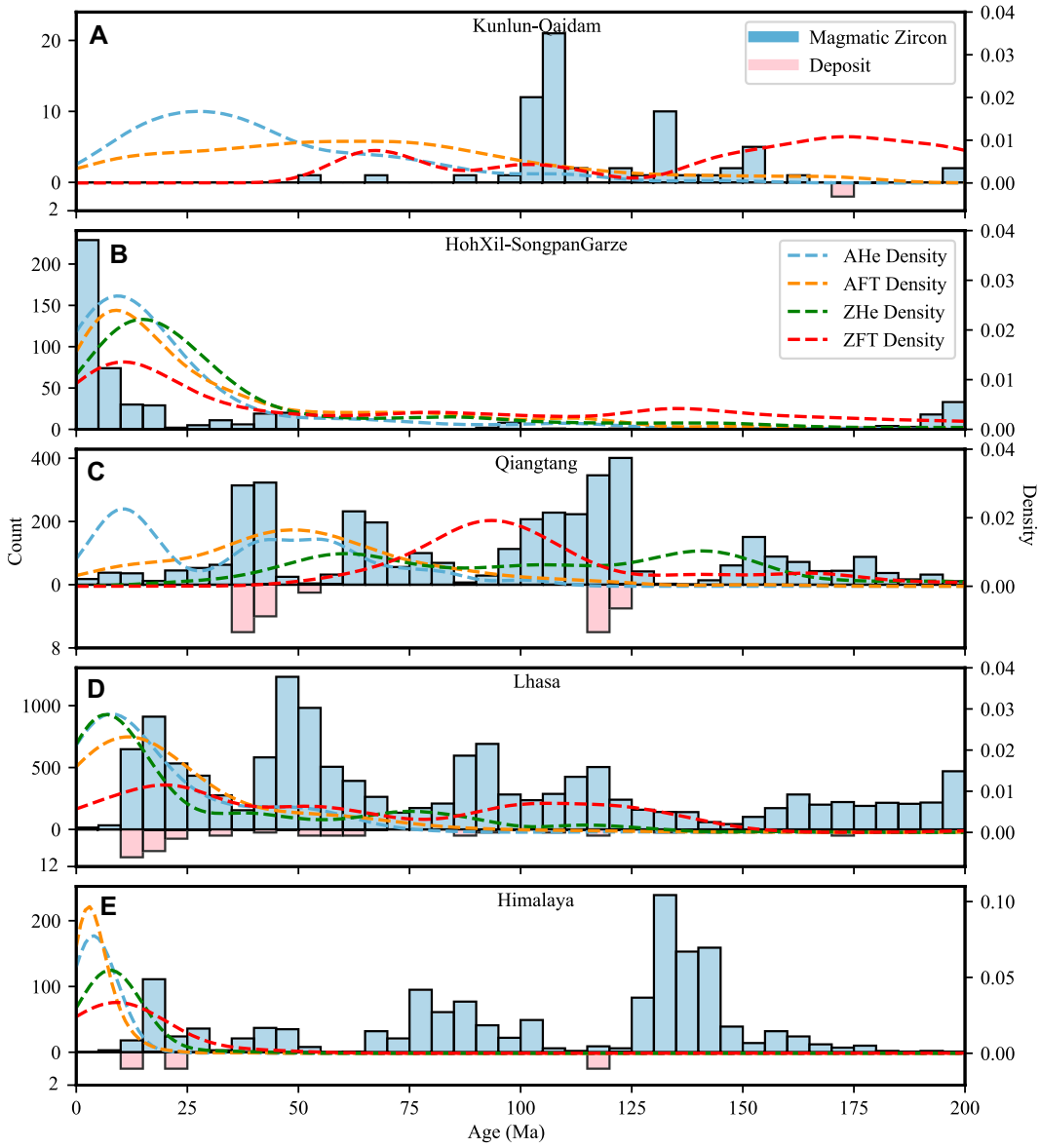

Figure 2. Spatiotemporal distribution map of tectonic activity, magmatic events, and ore deposit distribution on the Tibetan Plateau since the Jurassic. The dashed curve illustrates the kernel density distribution of thermochronological data, serving as an indicator of tectonic activity intensity. The blue histogram shows the distribution of magmatic zircon counts, which reflects the abundance of magmatic activity. The pink histogram represents the number of ore deposits, highlighting mineralization processes. AFT—apatite fission-track; Ahe—apatite (U-Th)/He; ZFT—zircon fission-track; ZHe—zircon (U-Th)/He.

extent, as an inheritance of the Triassic orogeny (Indosinian Orogeny; Roger et al., 2010).

During the early Cretaceous, the collision between the Lhasa and Qiangtang terranes triggered widespread magmatic activity within both terranes (Figs. 2C and 2D). Before this, the closure of the Paleo-Tethys Ocean caused two stages of bidirectional subduction of the Bangong-Nujiang Tethys oceanic lithosphere, resulting in a prolonged Jurassic magmatic record in the Lhasa and Qiangtang terranes (Zhu et al., 2016; Li et al., 2020; Liu et al., 2022). The scarcity of magmatic records in the Qiangtang terrane between ca. 140 Ma and 130 Ma is interpreted as reflecting the termination of subduction and the initiation of collision (Kapp et al., 2007; Zhu et al., 2016). The relatively intense tectonic activity in the Lhasa and Qiangtang terranes during this period (Figs. 2C and 2D) can also be attributed to the closure of the Bangong Ocean. From the Early to mid-Cretaceous, driven by the northward flat-slab subduction of the Neo-Tethyan oceanic lithosphere, the Lhasa terrane subducted beneath the Qiangtang terrane. This led to significant crustal thickening and surface uplift in central Tibet even before the India-Eurasia continental collision (Kapp et al., 2007; Rohrmann et al., 2012; Zhang et al., 2019). However, Ma et al. (2021), by estimating mantle potential pressures, suggested that the continental lithosphere beneath central Tibet was relatively thin during the Late Cretaceous (ca. 90 Ma). They proposed that lithospheric delamination caused by excessive thickening in northern Qiangtang led to lithospheric stratification, which explains the lack of contemporaneous crustal shortening and related deformation in the Qiangtang terrane compared to the Lhasa terrane (Kapp and DeCelles, 2019). The subduction of the Lhasa terrane beneath the Qiangtang terrane may also account for the absence of magmatic records in the Qiangtang terrane and the eruption of magmatic activity in the Lhasa terrane during 95–85 Ma (Figs. 2C and 2D). The ca. 65 Ma India-Eurasia collision further intensified magmatic and tectonic activity in the Lhasa terrane. Simultaneously, the collision sustained the convergence and compression of the Lhasa-Qiangtang terrane, resulting in crustal shortening and thickening in the Qiangtang terrane (Kapp et al., 2007; Rohrmann et al., 2012; Zhao et al., 2020), which may have suppressed volcanic activity. During 55–45 Ma, the breakoff of the Neo-Tethyan oceanic plate beneath

the Lhasa terrane triggered magmatic eruptions in the Gangdese Arc (Zhu et al., 2017; Kapp and DeCelles, 2019). The continued northward subduction of the Indian lithosphere terminated magmatic activity in southern Lhasa by ca. 40 Ma (DeCelles et al., 2011). From 45 Ma to 30 Ma, magmatic activity in the Qiangtang terrane increased in intensity, influenced by the continued southward subduction of the Asian lithosphere and the northward subduction and delamination of the Lhasa lithosphere (Ding et al., 2003, 2007, 2022; Guo and Wilson, 2019; Fig. 2C). Around 25 Ma, delamination and faulting in the Eurasian and Indian plates respectively caused tectonic and magmatic activity in southern Tibet (Lhasa) and northern Tibet (Hoh Xil Basin; Ding et al., 2022). The onset of frequent magmatic activity in Hoh Xil is linked to the break-off of the Asian lithosphere beneath the Hoh Xil Basin (Fig. 2B). After the dense segment of the Indian plate broke off, the relatively cold Indian lithosphere resumed northward subduction. Consequently, magmatic activity in southern Tibet has been in decline since 8 Ma (Ding et al., 2022).

Figure 2E shows that the Himalayan terrane has undergone three significant magmatic events. These correspond to (1) a large igneous province event in the eastern Tethys Himalaya during the Early Cretaceous triggered by the Kerguelen mantle plume (Zhu et al., 2008, 2009; Xia et al., 2014b; Ma et al., 2018), (2) magmatism induced by the rollback of subducted Neo-Tethys oceanic crust at ca. 90 Ma (Ma et al., 2013a, 2013b; Wan et al., 2019), and (3) magmatism triggered by the lithospheric break-off of the Indian plate at ca. 25 Ma (Chen et al., 2015; Ji et al., 2020; Ding et al., 2022). The continued subduction of the Indian lithosphere beneath the southern Himalaya eventually terminated magmatic activity in the Himalayan terrane (Ding et al., 2022). Intense tectonic denudation has resulted in the preservation of only thermochronological data younger than ca. 25 Ma in the Himalaya (Fig. 2E), reflecting the rapid elevation of the Himalayan terrane. It should be noted that the Himalayan orogen is a Cenozoic feature formed by the India-Eurasia collision. Thus, the pre-Cenozoic magmatic events (1 and 2) predate the orogeny and fall outside the focus of this study; they are presented solely to provide a complete record of magmatic activity.

4.2. Paleoelevation of the Tibetan Plateau

Figure 3 displays the correlation results between the crustal thickness calculated using the extremely randomized tree model and the actual crustal thickness (derived from CRUST1.0). The results indicate a good fit of the model. Therefore, this study considers the predicted crustal thickness using this method to be highly convincing. After obtaining the results for crustal thickness in the Tibetan Plateau, further simulated reconstructions of paleoelevation for the Southern Lhasa, Central and Northern Lhasa, and Qiangtang terranes were performed using transformation formulas. The reconstruction result is shown in Figure 4. Our paleoelevation reconstruction builds on previous work by incorporating broader spatial data coverage (see Fig. S1), extending the temporal range from the Jurassic to the present, and generating spatiotemporally explicit elevation ranges with median values. This refined reconstruction serves as a valuable extension and update to existing models of paleoelevation evolution. In this study, paleoelevation is used not as a standalone research focus but as a quantitative basis for examining its spatiotemporal relationship with porphyry deposits. This section provides the paleotopographic context for the analyses that follow.

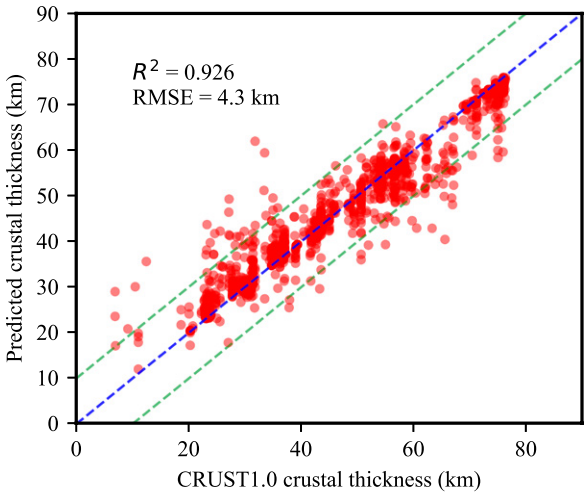

Figure 3. Comparison of crustal thickness predicted by extremely randomized tree model with that given by CRUST1.0 in validating the dataset. The coefficient of determination (R^2) provides an indication of goodness of fit, and the root-mean-square error (RMSE) is the standard deviation of the prediction error.

A comparison reveals that the reconstructed paleoelevation in this study generally aligns with the paleoelevation records found in the literature (Fig. 4). However, it is noteworthy that for certain periods and regions, the reconstructed results for some terranes are notably lower or higher than the majority of paleoelevation records, such as during the 65–30 Ma period for the Lhasa terrane. One potential reason for these discrepancies could be the regional distribution of magmatic rocks within the terrane during that period, where data cannot cover the entire terrane well, leading to reconstructed results reflecting only the paleoelevation history of specific local areas within the terrane rather than the entire region. Another possibility could be that the uplift of the terrane was regional and heterogeneous, while previous studies' paleoelevation records were concentrated in certain popular research areas, thereby not effectively constraining the entire terrane. This issue is particularly evident during the 65–45 Ma period for the Lhasa terrane, where the reconstructed paleoelevation results in this study exhibit a wide range of variations. These variations reflect the intense and heterogeneous tectonic activity and uplift history of the Lhasa terrane during the collision between the Indian and Eurasian plates, highlighting the challenges in accurately capturing the paleoelevation dynamics of the region during this period.

Our results indicate that during the Jurassic period, the paleoelevation of certain local areas within the Lhasa terrane may have fluctuated, but the average elevation remained nearly unchanged, consistently oscillating around sea level (Figs. 4A and 4B). In contrast, the average elevation of the Qiangtang terrane experienced a significant uplift of nearly 2000 m during the Late Jurassic (Fig. 4C), influenced by the northward subduction of the Bangong-Nujiang Tethys Ocean. However, prior to its collision with the Lhasa terrane, the average elevation of the Qiangtang terrane returned to ~1000 m. This was likely due to the bidirectional subduction of the Bangong-Nujiang Tethys, which created a widespread extensional environment in the lithosphere (Li et al., 2024). Between ca. 120 Ma and 100 Ma, the collision between the northern Lhasa terrane and the Qiangtang terrane caused an uplift of ~1600 m in the central and northern Lhasa terrane. Although the average elevation of the Qiangtang terrane showed no significant change during this period, the presence of elevation anomalies reflects localized uplift events in certain areas. This phenomenon could be attributed to crustal thickening within the Qiangtang terrane, induced by the collision, which subsequently led to lithospheric delamination over a short time scale (please see Section 4.1). The effects of this collision persisted

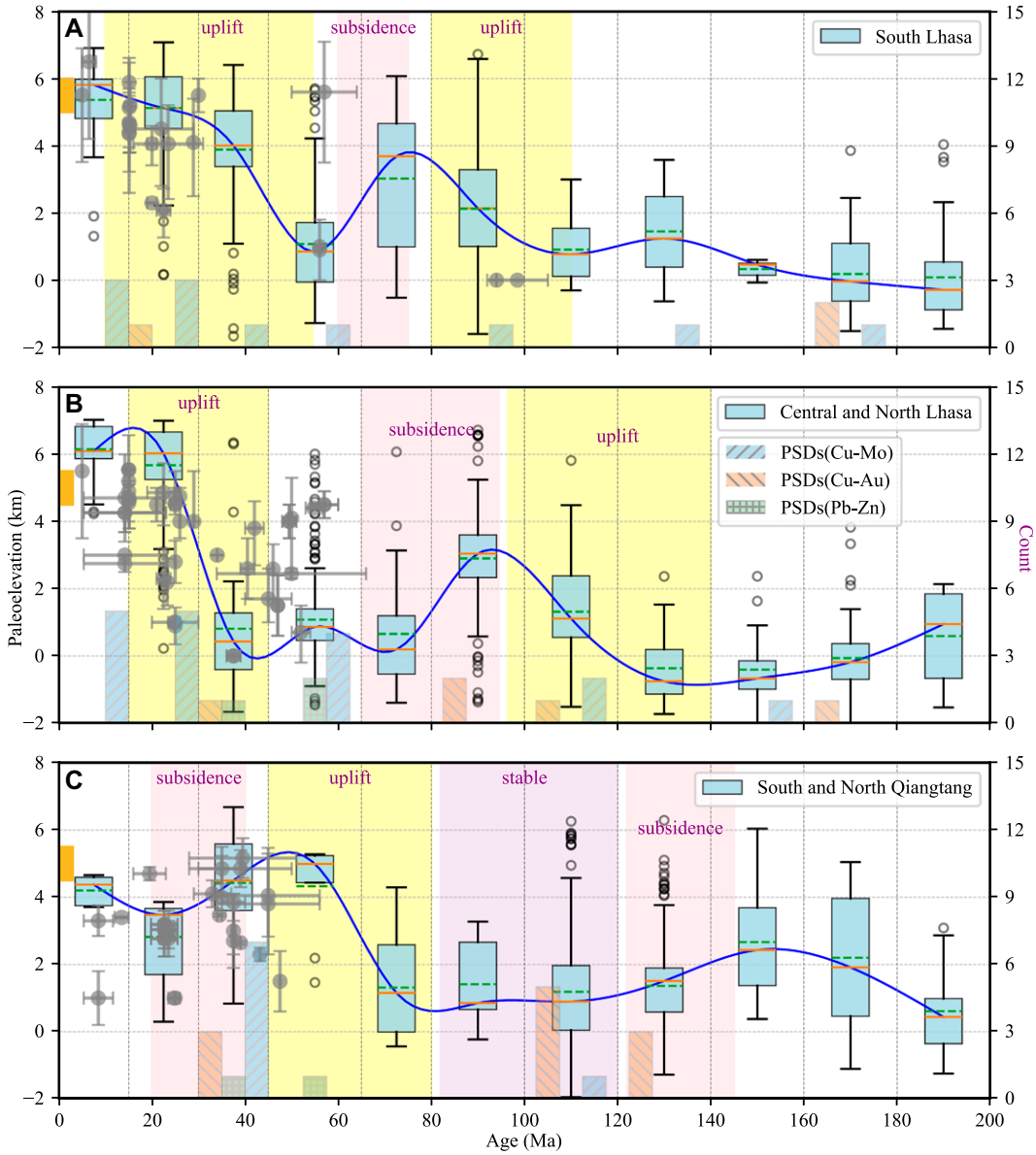

Figure 4. Reconstruction of paleoelevation in the Tibetan Plateau. The collection of regional paleoelevations every 15 m.y. or 20 m.y. The results reconstructed in this paper are represented by box plots, where the orange solid line represents the median and the green dashed line represents the average. The hollow circles represent outliers in the box plots. The solid blue line connects the medians of paleoelevation for each time period, simulating the temporal variation in paleoelevation. The gray dots indicate paleoelevation records from the literature, while the colored histogram represents the number of newly formed porphyry deposits during that time period. The orange range on the left *y*-axis denotes the current elevation range of the region. PSDs—porphyry system deposits.

into the 100–80 Ma period, during which the average elevation of the central and northern Lhasa terrane rose to ~2800 m, with the uplift extending southward. This southward extension resulted in the southern Lhasa terrane reaching a paleoelevation of ~3000 m before the collision between India and Eurasia. Before 65 Ma, the average elevation of the central and northern Lhasa terrane returned to its Jurassic level, which may be linked to slab rollback preceding the break-off of the Neo-Tethyan oceanic lithosphere (Manea et al., 2012; Hu et al., 2020). This extensional regime extended into the southern Lhasa terrane during the initial stages of the India–Asia collision. Another possibility is that excessive crustal thickening in the Lhasa terrane led to lithospheric delamination during the Late Cretaceous; however, this event likely occurred later than the delamination experienced by the Qiangtang terrane (Ji et al., 2014).

The widespread anomalies observed in Figures 4A and 4B during the 65–45 Ma period reflect an unstable paleo-elevation history of the Lhasa terrane in the early stages of the collision. However, the average elevation of the Lhasa terrane during this time shows no significant overall uplift. Following the break-off of the Neo-Tethyan oceanic plate beneath southern Tibet, which triggered magmatic activity (Zhu et al., 2017; Kapp and DeCelles, 2019), southern Lhasa experienced rapid uplift. By the 45–30 Ma period, its average elevation had reached ~4000 m. During this same period, the northward subduction of the Indian lithosphere terminated magmatic activity in southern Lhasa (DeCelles et al., 2011), leading to a subsequent slowdown in the uplift rate (Fig. 4A). In contrast, the average elevation of central and northern Lhasa remained ~1000 m since 80 Ma, until a period of rapid uplift occurred during 40–30 Ma. This uplift was triggered by the delamination and break-off of the Lhasa lithospheric mantle due to subduction processes (Ding et al., 2003, 2007, 2022; Guo and Wilson, 2019). As revealed by our study, the relatively low elevations of the Qiangtang and central-northern Lhasa terranes prior to the India-Eurasia collision support the view proposed by Guo et al. (2025) that the north-central Tibetan Plateau experienced extensive crustal thickening during the Cenozoic. Overall, from 30 Ma to the present, the Lhasa

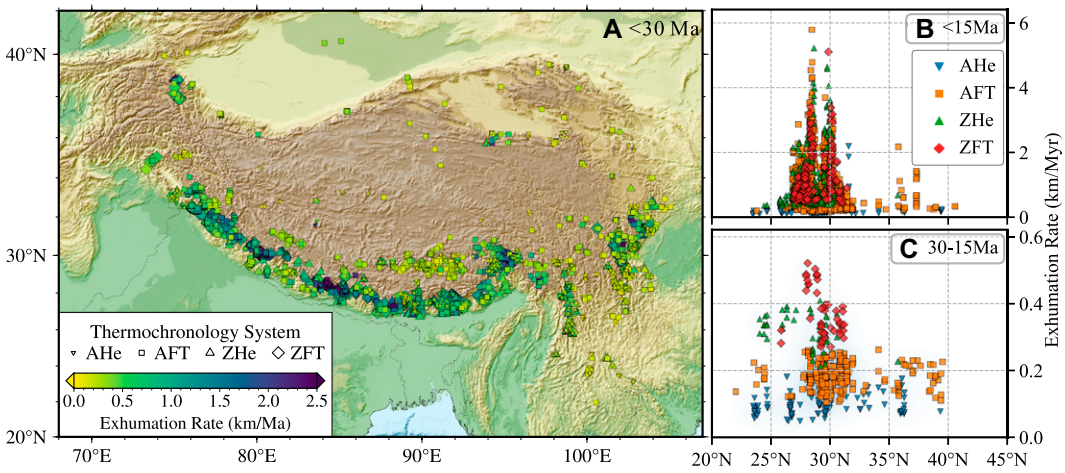

Figure 5. The calculated results of exhumation rate. (A) The spatial distribution of exhumation rates. (B, C) The latitudinal distribution of exhumation rates calculated using apatite (U-Th)/He (Ahe), apatite fission-track (AFT), zircon (U-Th)/He (ZHe), and zircon fission-track (ZFT) data. The blue shading represents the kernel density distribution of exhumation rate calculation results.

terrane has undergone continuous uplift, gradually reaching its current elevation. As for the Qiangtang terrane, two distinct stages of uplift can be identified since the collision between India and Eurasia. The first stage was an early uplift phase driven by crustal thickening associated with the collision. The second stage, we propose, was triggered by the delamination of the Asian lithospheric mantle beneath the Qiangtang terrane ca. 25 Ma (Zhao et al., 2020, 2022b; Li et al., 2022).

4.3. Regional Exhumation of the Plateau

The preservation of porphyry deposits is primarily influenced by arid paleoclimate conditions and Cenozoic tectonic quiescence (Gong et al., 2021). The exhumation of the Tibetan Plateau is controlled by the interplay between tectonics and climate, as well as their coupling effects (Copeland et al., 1995; Willett, 1999). Tectonics drive rock uplift and exhumation, while climate enhances erosion rates, removing surface materials. Notably, the intensification of the Asian monsoon during the mid-Miocene (ca. 15–10 Ma) played a dominant role in the exhumation of the Tibetan Plateau region (Clift et al., 2008). This intensification likely influenced hydrothermal activity and material migration within porphyry systems by altering moisture conditions and mineral compositions in the crust. Furthermore, the differential exhumation of the Tibetan Plateau affects the exposure levels of overlying strata and even the porphyry bodies themselves (Leng et al., 2018), which is critical for the subsequent preservation of ore deposits. Therefore, quantifying the differential exhumation of the Tibetan Plateau is essential for understanding regional mineralization processes and the preservation of deep-seated ore deposits.

The strong influence of the Asian monsoon has led to a sharp increase in the exhumation rate of the Tibetan Plateau since ca. 15 Ma (Clift et al., 2008). Additionally, considering the uncertainty of paleogeothermal gradients and the limited availability of older data, which may result in larger errors, we have restricted our discussion to the exhumation rates calculated for the past 30 m.y. We found that, since 30 Ma, the exhumation rate in the southern plateau has been significantly higher than that in the northern plateau, with the highest exhumation rate observed near 30°N latitude (Figs. 5B and 5C). This corresponds to the Gangdese region south of Lhasa and the Himalayan orogenic belt (Fig. 5A). Subsequently, we calculated the exhumation thickness using the exhumation rate and corresponding thermochronological ages. The calculated results were subjected to kriging interpolation, which allowed us to obtain the distribution of exhumation thickness across different regions of the Tibetan Plateau since 30 Ma (Fig. 6). These results are well correlated with tectonic events in the Tibetan Plateau. The Qaidam terrane, the Songpan-Ganzi terrane, the Hoh Xil Basin, and the Lhasa region exhibit extensive and thick exhumation (Fig. 6), which are respectively associated with the southward subduction of the Qaidam terrane ca. 30 Ma (Tapponnier et al., 2001; Ding et al., 2003; Ye et al., 2015; Qi et al., 2020), the impact of the India-Asia continental collision ca. 30 Ma on the Songpan-Ganzi terrane (Xu and Kamp, 2000; Jolivet et al., 2001; Wilson et al., 2006; Roger et al., 2010), and the delamination and faulting beneath the Lhasa and Hoh Xil Basin ca. 25 Ma (Ding et al., 2022; please see Section 4.1 for more details). Furthermore, since 15 Ma, the exhumation rate along the Himalayan topographic front has been exceptionally high (Clift et al., 2008), resulting in the thickest exhumation depths in the Himalayan region (Fig. 6).

Since 30 Ma, the Tibetan Plateau has been subjected to continuous denudation driven by active tectonic processes (Fig. 2), aligning well with the conditions assumed in this study and the applied model. However, it is important to emphasize that the model assumes a constant denudation rate, which clearly underestimates the temporal variability of denudation rates over geological time scales. On the other hand, while we employed different input parameters for different time intervals during model application, we still assumed that the parameters remained constant within each specific time interval, which is likewise a coarse approximation. Consequently, the calculated denudation rates and thicknesses presented in this study inevitably involve some degree of error. Fortunately, the primary focus of this study lies in the spatial variations of denudation across different regions. Since the model exerts similar effects on all predicted regions, we are confident that the results are valid for the purpose of cross-regional comparisons of denudation magnitude. To achieve more accurate estimations of regional denudation volumes and rates, we recommend incorporating more comprehensive datasets and employing more advanced simulation software.

4.4. Indication of the Distribution of Porphyry Deposits

PSDs within Jurassic-aged rocks of the Tibetan Plateau are primarily concentrated in the Qiangtang terrane, the Lhasa terrane, and the southeastern margin of the plateau (Fig. 1). Examining the temporal distribution of deposits in Figure 2, we observe that PSDs in the Lhasa terrane are predominantly distributed across three time intervals: 180–165 Ma, 120–85 Ma, and 65–10 Ma. In contrast, PSDs in the Qiangtang terrane are mainly distributed during 125–115 Ma and 45–30 Ma. These time periods correspond to major tectonic events, such as the bidirectional subduction of the Bangong-

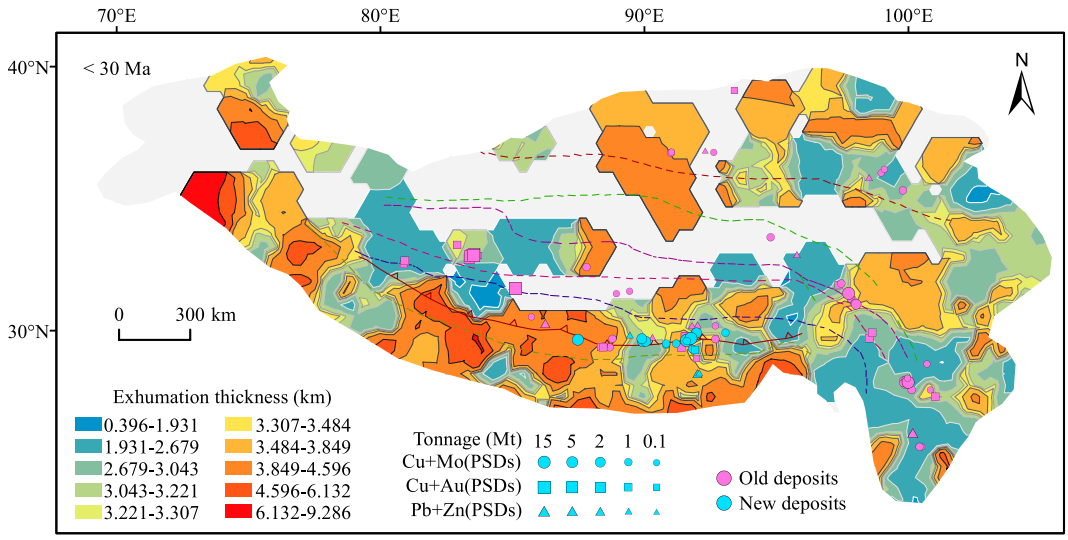

Figure 6. Kriging interpolation of exhumation thickness in the Tibetan Plateau. Exhumation thickness = exhumation rate × thermochronology age. The circular symbols represent the types of mineral deposits, while the size of the symbols indicates the tonnage of the deposits. Blue symbols represent newly formed deposits within the current time range (deposit age after 30 Ma), whereas pink symbols indicate older deposits formed prior to the time period (deposit age before 30 Ma). All kriging interpolations were performed in ArcGIS. PSDs—porphyry system deposits.

Nujiang Tethys, the collision of the Lhasa and Qiangtang terranes, and the India-Eurasia continental collision. Without exception, these events triggered significant tectonic and magmatic episodes, which are prerequisites for the formation of PSDs. To ultimately form porphyry deposits, the magma must exhibit relatively high oxygen fugacity, and sulfur and water content (Sillitoe, 2010; Richards, 2015), as these factors determine the metallogenic fertility of the magma. Despite abundant magmatic activity in the East Kunlun region ca. 110 Ma, typical porphyry copper systems did not develop (Fig. 2A). This is attributed to the relatively low oxygen fugacity and water content of the associated magma (Feng et al., 2024).

In addition to tectonic and magmatic activity, the formation of PSDs is closely linked to crustal thickness, as well as active uplift and erosion (Richards, 2003; Cooke et al., 2005; Wilkinson, 2013; Lee and Tang, 2020). By analyzing the number of various types of deposits in the Lhasa and Qiangtang terranes over different time intervals and comparing these with paleoelevation evolution trends, we find that most porphyry deposits in the Tibetan Plateau developed during periods of significant paleoelevation changes. During these periods, the paleoelevation of the Lhasa and Qiangtang terranes exhibited rapid increases or decreases, or regional instability, which is reflected in the increasing frequency of outliers (Fig. 4). We attribute this to the controlling role of crustal thickness in ore formation. Paleoelevation changes result from both tectonic evolution and surface fluctuations. In this study, we only consider the control of tectonic evolution on paleoelevation, simplifying the relationship between paleoelevation and crustal thickness to a linear model under idealized conditions. Here, paleoelevation serves as a key proxy that translates deep crustal thickness changes into an interpretable surface-topographic narrative. This transformation allows us to directly link orogenic evolution with near-surface processes (e.g., exhumation), thereby explaining the spatial distribution of deposits. While this simplification overlooks surface processes to some extent, it still highlights the importance of crustal thickness in controlling the development of PSDs. Crustal thickness influences the duration and volume of magmatic activity, the timing of sulfide saturation, and the enrichment of chalcophile elements (Park et al., 2021; Chiaradia, 2022). Furthermore, magmas tend to exhibit higher oxygen fugacity with increasing crustal thickness (Wilkinson, 2013; Richards, 2015; Ai et al., 2025). Thus, crustal thickness plays a critical role in the development of PSDs, which partially explains the relationship between paleoelevation evolution and the temporal distribution of PSDs observed in this study.

When comparing the distribution of PSDs between the Lhasa terrane and the Qiangtang terrane, it is evident that the Qiangtang terrane hosts a greater number of porphyry Cu-Au deposits, which are primarily associated with the extensional stages of the terrane. In contrast, the Lhasa terrane predominantly features porphyry Cu(-Mo) deposits, mostly formed during periods of paleoelevation uplift (Fig. 4). This observation highlights the influence of crustal thickness on the metallogenic processes of porphyry systems. Specifically, porphyry Cu deposits enriched in copper are more likely to form in regions with a thickened lower crust. This is because the development of large, water-rich magma chambers in the deep middle to lower crust can supply adequate amounts of Cu (Cooke et al., 2005; Chiaradia and Caricchi, 2017; Park et al., 2021; Richards, 2022). On the other hand, thinner crusts, which may receive a greater influx of oxidized materials from subducted slabs, tend to exhibit higher oxidation states. This leads to early sulfide saturation, resulting in the depletion of copper at earlier stages (Jenner et al., 2010; Park et al., 2015, 2019; Lee and Tang, 2020; Ai et al., 2025). However, the late-stage sulfide saturation in shallow magma reservoirs, combined with an increase in chalcophile elements, enhances the precipitation efficiency of gold in fluids. Consequently, thinner crusts have a relatively greater potential for hosting gold-rich porphyry copper deposits (Chiaradia, 2020, 2022). Figure 4 further reflects the differing mechanisms of deposit formation between the two terranes: the southern Lhasa terrane is dominated by crustal thickening–related mineralization, whereas the Qiangtang terrane is primarily characterized by crustal thinning–related mineralization. In the central and northern Lhasa terrane, both mechanisms are evident. We attribute these differences to the tectonic settings of the subduction margins of the continental plates. Subduction margins undergo rapid thickening during continental collision, while post-collision, they are more likely to experience extensional tectonic regimes. Additionally, excessive crustal thickening at the subduction margins during collision can lead to crustal delamination, resulting in crustal thinning. We propose that the collision between the Lhasa and Qiangtang terranes, as well as the collision between the Indian and Asian plates, caused over-thickening and subsequent delamination at the subduction margins (please see Section 4.1). This process facilitated the ascent of magma into the overlying central and northern Lhasa terrane and the

Qiangtang terrane, forming PSDs in an extensional setting. In contrast, the southern Lhasa terrane, influenced by the persistent northward push of the Indian plate and the stress transmitted from the northern collision, remained under compressional conditions during continental collision. As a result, magmatic ascent and mineralization in the southern Lhasa terrane were often accompanied by crustal thickening.

Notably, the number of newly formed deposits in the Lhasa terrane surged during the 25–10 Ma period, but no new PSDs have developed since 10 Ma (Fig. 2D). This phenomenon can be attributed to the delamination and fracturing of the Asian and Indian continental lithospheres ca. 25 Ma, which triggered intense tectonic and magmatic activity in southern Tibet (Lhasa) and northern Tibet (Hoh Xil Basin; Ding et al., 2003). In the Lhasa terrane, magmatic activity was terminated ca. 8 Ma due to the renewed subduction of the Indian plate (please see Section 4.1), effectively halting the formation of porphyry deposits. In contrast, despite experiencing similar tectonic and magmatic processes since 25 Ma, the Hoh Xil–Songpan Garze terrane did not develop any PSDs (Fig. 2B). We hypothesize that this may be related to the significant exhumation experienced in the Hoh Xil–Songpan Garze region since ca. 15 Ma.

By integrating the exhumation thickness distribution across the Tibetan Plateau, as calculated in this study, with the distribution of PSDs (Fig. 6), we observe that the vast majority of deposits are concentrated in areas with relatively low exhumation thickness. In contrast, deposits located in regions with higher exhumation thickness tend to have relatively smaller tonnages. We interpret this pattern as evidence that the shallow burial depth of porphyry deposits (typically 1–6 km) makes regions with extensive exhumation less favorable for both the formation and subsequent preservation of such deposits. Among the three major porphyry metallogenic belts of the Tibetan Plateau, both the Bangong-Nujiang and Yulong metallogenic belt are located in regions of relatively low exhumation. In the Gangdese belt, the eastern and western segments similarly exhibit limited exhumation, whereas the central segment shows significantly higher exhumation levels. However, due to the lack of thermochronological data in the central and western segments of the Gangdese belt, the calculated exhumation rates in these regions are limited (Fig. 5A), which may affect the precision of the interpolated results in Figure 6. A similar situation is observed in the Hoh Xil region. To better constrain the extent of exhumation in the central and western Gangdese, additional thermochronological data are required. In conclusion, we conclude that the formation of PSDs requires intense tectonic and magmatic activities, while a lower degree of exhumation is equally important for their subsequent preservation. Porphyry deposits formed in regions that have experienced intense erosion since 30 Ma may have already been eroded away. Conversely, regions with extremely low exhumation thickness are also associated with sparse mineral deposit distributions (Fig. 6). We hypothesize that this may be due to limited excavation in these areas, with mineral deposits likely remaining buried at greater depths and yet to be discovered. These regions could serve as key targets for future mineral exploration.

5. CONCLUSIONS

This study reconstructs the tectonic activity, magmatic evolution, and paleoelevation variations and exhumation history of different tectonic terranes of the Tibetan Plateau from the Jurassic to the present, based on extensive datasets including whole-rock geochemistry of magmatic rocks, zircon geochronology, and low-temperature thermochronology. Our findings refine the understanding of the tectonic and topographic history of the Tibetan Plateau and provide robust constraints on the formation and subsequent preservation of PSDs. The main conclusions are as follows:

(1) Regions with intense exhumation host fewer PSDs and deposits with relatively smaller tonnages, indicating that such environments are not conducive to the subsequent preservation of porphyry deposits. In certain regions with relatively low degrees of erosion, mineral deposits may remain buried at considerable depths and have yet to be discovered, thus representing key targets for future mineral exploration.

(2) The distinct metallogenic mechanisms between the Lhasa and Qiangtang terranes are attributed to their respective positions along the subduction fronts of different continental plates. In the southern Lhasa terrane, porphyry mineralization formed during intervals of crustal thickening, which are generally associated with higher paleoelevation tendencies, whereas in the Qiangtang terrane, it is mainly linked to crustal thinning and correspondingly lower paleoelevation tendencies. In contrast, the central and northern parts of the Lhasa terrane exhibit the coexistence of both mechanisms. Moreover, the differences in PSD types between the two terranes suggest that a thicker crust facilitates greater Cu supply to porphyry systems, while a thinner crust favors Au enrichment.

ACKNOWLEDGMENTS

This work was supported by the National Key R&D Program of China (grant 2023YFC2906402), the National Natural Science Foundation of China (grants 42430111, 42472358, 42595552, and 42050103), Guangdong Province Introduced Innovative R&D Team of Big Data–Mathematical Geosciences and Extreme Geological Events Team (grant 2021ZT09H399), and the Fundamental Research Funds for the Central Universities (grant 2652023001).

REFERENCES CITED

Ai, Y., Chiaradia, M., Wu, C., and Chen, H., 2025, Crustal magma oxidation state and endowments in porphyry copper deposits: Science China Earth Sciences, v. 68, p. 226–236, https://doi.org/10.1007/s11430-024-1429-6 [in Chinese with English abstract].

Allégre, C.J., et al., 1984, Structure and evolution of the Himalaya–Tibet orogenic belt: Nature, v. 307, p. 17–22, https://doi.org/10.1038/307017a0.

An, Z., Kutzbach, J.E., Prell, W.L., and Porter, S.C., 2001, Evolution of Asian monsoons and phased uplift of the Himalaya–Tibetan plateau since Late Miocene times: Nature, v. 411, p. 62–66, https://doi.org/10.1038/35075035.

Bierlein, F.P., Reynolds, N., Arne, D., Bargmann, C., McKeag, S., Bullen, W., Al-Athbah, H., McKnight, S., and Maas, R., 2016, Petrogenesis of a Neoproterozoic magmatic arc hosting porphyry Cu-Au mineralization at Jebel Ohier in the Gebeit Terrane, NE Sudan: Ore Geology Reviews, v. 79, p. 133–154, https://doi.org/10.1016/j.oregeorev.2016.05.010.

Black, L.P., Kamo, S.L., Williams, I.S., Mundil, R., Davis, D.W., Korsch, R.J., and Foudoulis, C., 2003, The application of SHRIMP to Phanerozoic geochronology; a critical appraisal of four zircon standards: Chemical Geology, v. 200, p. 171–188, https://doi.org/10.1016/S0009-2541(03)00166-9.

Cao, K., Tian, Y., van der Beek, P., Wang, G., Shen, T., Reiners, P., Bernet, M., and Husson, L., 2022, Southwestward growth of plateau surfaces in eastern Tibet: Earth-Science Reviews, v. 232, https://doi.org/10.1016/j.earscirev.2022.104160.

Cavosie, A.J., Wilde, S.A., Liu, D., Weiblen, P.W., and Valley, J.W., 2004, Internal zoning and U–Th–Pb chemistry of Jack Hills detrital zircons: A mineral record of early Archean to Mesoproterozoic (4348–1576 Ma) magmatism: Precambrian Research, v. 135, p. 251–279, https://doi.org/10.1016/j.precamres.2004.09.001.

Chapman, J.B., and Kapp, P., 2017, Tibetan magmatism database: Geochemistry, Geophysics, Geosystems, v. 18, p. 4229–4234, https://doi.org/10.1002/2017GC007217.

Chen, Y., Li, W., Yuan, X., Badal, J., and Teng, J., 2015, Tearing of the Indian lithospheric slab beneath southern Tibet revealed by SKS-wave splitting measurements: Earth and Planetary Science Letters, v. 413, p. 13–24, https://doi.org/10.1016/j.epsl.2014.12.041.

Chiaradia, M., 2020, Gold endowments of porphyry deposits controlled by precipitation efficiency: Nature Communications, v. 11, 248, https://doi.org/10.1038/s41467-019-14113-1.

Chiaradia, M., 2022, Distinct magma evolution processes control the formation of porphyry Cu–Au deposits in thin and thick arcs: Earth and Planetary Science Letters, v. 599, https://doi.org/10.1016/j.epsl.2022.117864.

Chiaradia, M., and Caricchi, L., 2017, Stochastic modelling of deep magmatic controls on porphyry copper deposit endowment: Scientific Reports, v. 7, https://doi.org/10.1038/srep44523.

Clark, M.K., and Royden, L.H., 2000, Topographic ooze: Building the eastern margin of Tibet by lower crustal flow: Geology, v. 28, p. 703–706, https://doi.org/10.1130/0091-7613(2000)28<703:TOBTEM>2.0.CO;2.

Clark, M.K., House, M.A., Royden, L.H., Whipple, K.X., Burchfiel, B.C., Zhang, X., and Tang, W., 2005, Late Cenozoic uplift of southeastern Tibet: Geology, v. 33, p. 525–528, https://doi.org/10.1130/G21265.1.

Clift, P.D., Hodges, K.V., Heslop, D., Hannigan, R., Van Long, H., and Calves, G., 2008, Correlation of Himalayan exhumation rates and Asian monsoon intensity: Nature Geoscience, v. 1, p. 875–880, https://doi.org/10.1038/ngeo351.

Cooke, D.R., Hollings, P., and Walshe, J.L., 2005, Giant porphyry deposits: Characteristics, distribution, and tec-

tonic controls: Economic Geology, v. 100, p. 801–818, https://doi.org/10.2113/gsecongeo.100.5.801.

Copeland, P., Harrison, T.M., Pan, Y., Kidd, W.S.F., Roden, M., and Zhang, Y., 1995, Thermal evolution of the Gangdese batholith, southern Tibet: A history of episodic unroofing: Tectonics, v. 14, p. 223–236, https://doi.org/10.1029/94TC01676.

Craddock, W.H., Kirby, E., Dewen, Z., and Jianhui, L., 2012, Tectonic setting of Cretaceous basins on the NE Tibetan Plateau: Insights from the Jungong basin: Basin Research, v. 24, p. 51–69, https://doi.org/10.1111/j.1365-2117.2011.00515.x.

DeCelles, P.G., Kapp, P., Quade, J., and Gehrels, G.E., 2011, Oligocene–Miocene Kailas basin, southwestern Tibet: Record of postcollisional upper-plate extension in the Indus-Yarlung suture zone: Geological Society of America Bulletin, v. 123, p. 1337–1362, https://doi.org/10.1130/B30258.1.

Ding, L., Kapp, P., Zhong, D., and Deng, W., 2003, Cenozoic volcanism in Tibet: Evidence for a transition from oceanic to continental subduction: Journal of Petrology, v. 44, p. 1833–1865, https://doi.org/10.1093/petrology/egg061.

Ding, L., Kapp, P., Yue, Y., and Lai, Q., 2007, Postcollisional calc-alkaline lavas and xenoliths from the southern Qiangtang terrane, central Tibet: Earth and Planetary Science Letters, v. 254, p. 28–38, https://doi.org/10.1016/j.epsl.2006.11.019.

Ding, L., Xu, Q., Yue, Y., Wang, H., Cai, F., and Li, S., 2014, The Andean-type Gangdese Mountains: Paleoelevation record from the Paleocene–Eocene Linzhou Basin: Earth and Planetary Science Letters, v. 392, p. 250–264, https://doi.org/10.1016/j.epsl.2014.01.045.

Ding, L., Spicer, R.A., Yang, J., Xu, Q., Cai, F., Li, S., Lai, Q., Wang, H., Spicer, T.E.V., Yue, Y., Shukla, A., Srivastava, G., Khan, M.A., Bera, S., and Mehrotra, R., 2017, Quantifying the rise of the Himalaya orogen and implications for the South Asian monsoon: Geology, v. 45, p. 215–218, https://doi.org/10.1130/G38583.1.

Ding, L., Kapp, P., Cai, F., Garzione, C.N., Xiong, Z., Wang, H., and Wang, C., 2022, Timing and mechanisms of Tibetan Plateau uplift: Nature Reviews: Earth & Environment, v. 3, p. 652–667, https://doi.org/10.1038/s43017-022-00318-4.

Dupont-Nivet, G., Krijgsman, W., Langereis, C.G., Abels, H.A., Dai, S., and Fang, X., 2007, Tibetan plateau aridification linked to global cooling at the Eocene–Oligocene transition: Nature, v. 445, p. 635–638, https://doi.org/10.1038/nature05516.

Farley, K.A., and Stockli, D.F., 2002, (U-Th)/He dating of phosphates: Apatite, monazite, and xenotime: Reviews in Mineralogy and Geochemistry, v. 48, p. 559–577, https://doi.org/10.2138/rmg.2002.48.15.

Feng, C., Wang, H., Qu, H., Yu, M., and Zhong, S., 2024, Paleo-Tethys tectonic evolution and related large-scale metallogenic features in East Kunlun Orogen: Mineralium Deposita, v. 43, no. 6, p. 1316–1335 [in Chinese with English abstract].

Fielding, E., Isacks, B., Barazangi, M., and Duncan, C., 1994, How flat is Tibet?: Geology, v. 22, p. 163–167, https://doi.org/10.1130/0091-7613(1994)022<0163:HFIT>2.3.CO;2.

Gong, L., Kohn, B.P., Zhang, Z., Xiao, B., Wu, L., and Chen, H., 2021, Exhumation and Preservation of Paleozoic Porphyry Cu Deposits: Insights from the Yandong Deposit, Southern Central Asian Orogenic Belt: Economic Geology, v. 116, p. 607–628, https://doi.org/10.5382/econgeo.4812.

Guo, P., and Yang, T., 2023, Quantifying continental crust thickness using the machine learning method: Journal of Geophysical Research: Solid Earth, v. 128, https://doi.org/10.1029/2022JB025970.

Guo, P., Yang, T., and Ji, W., 2025, Linking Cenozoic magmatism in the north-central Tibetan Plateau with plateau growth: Geochemistry, Geophysics, Geosystems, v. 26, https://doi.org/10.1029/2024GC011898.

Guo, Z., and Wilson, M., 2019, Late Oligocene–early Miocene transformation of postcollisional magmatism in Tibet: Geology, v. 47, p. 776–780, https://doi.org/10.1130/G46147.1.

He, R., Liu, G., Golos, E., Gao, R., and Zheng, H., 2014, Isostatic gravity anomaly, lithospheric scale density structure of the northern Tibetan plateau and geodynamic causes for potassic lava eruption in Neogene: Tectonophysics, v. 628, p. 218–227, https://doi.org/10.1016/j.tecto.2014.04.047.

He, Z., et al., 2023, Low-temperature thermochronology of the Longmala-Mengya'a Pb-Zn deposits (southern Tibet): Implications for ore exhumation and preservation: Ore Geology Reviews, v. 160, https://doi.org/10.1016/j.oregeorev.2023.105611.

Hou, Z., Yang, Z., Lu, Y., Kemp, A., Zheng, Y., Li, Q., Tang, J., Yang, Z., and Duan, L., 2015, A genetic linkage between subduction- and collision-related porphyry Cu deposits in continental collision zones: Geology, v. 43, p. 247–250, https://doi.org/10.1130/G36362.1.

Hou, Z., et al., 2023, Formation of giant copper deposits in Tibet driven by tearing of the subducted Indian plate: Earth-Science Reviews, v. 243, https://doi.org/10.1016/j.earscirev.2023.104482.

Hu, F., Wu, F., Chapman, J.B., Ducea, M.N., Ji, W., and Liu, S., 2020, Quantitatively tracking the elevation of the Tibetan Plateau since the Cretaceous: Insights from whole-rock Sr/Y and La/Yb ratios: Geophysical Research Letters, v. 47, https://doi.org/10.1029/2020GL089202.

Hu, S., Cao, Y., Huang, J., and Mou, Z., 1999, Discussion on formation and evolution of Jurassic basin-prototype of Qaidam basin: Experimental Petroleum Geology, v. 21, no. 3, p. 189–195 [in Chinese with English abstract].

Hu, X., Garzanti, E., Wang, J., Huang, W., An, W., and Webb, A., 2016a, The timing of India-Asia collision onset—Facts, theories, controversies: Earth-Science Reviews, v. 160, p. 264–299, https://doi.org/10.1016/j.earscirev.2016.07.014.

Hu, X., Wang, J., BouDagher-Fadel, M., Garzanti, E., and An, W., 2016b, New insights into the timing of the India–Asia collision from the Paleogene Quxia and Jialazi formations of the Xigaze forearc basin, South Tibet: Gondwana Research, v. 32, p. 76–92, https://doi.org/10.1016/j.gr.2015.02.007.

Ibarra, D.E., et al., 2023, High-elevation Tibetan Plateau before India–Eurasia collision recorded by triple oxygen isotopes: Nature Geoscience, v. 16, p. 810–815, https://doi.org/10.1038/s41561-023-01243-x.

Ingalls, M., Rowley, D., Olack, G., Currie, B., Li, S., Schmidt, J., Tremblay, M., Polissar, P., Shuster, D.L., Lin, D., and Colman, A., 2018, Paleocene to Pliocene low-latitude, high-elevation basins of southern Tibet: Implications for tectonic models of India-Asia collision, Cenozoic climate, and geochemical weathering: Geological Society of America Bulletin, v. 130, p. 307–330, https://doi.org/10.1130/B31723.1.

Jenner, F.E.O., Neill, H.S.C., Arculus, R.J., and Mavrogenes, J.A., 2010, The magnetite crisis in the evolution of arc-related magmas and the initial concentration of Au, Ag and Cu: Journal of Petrology, v. 51, p. 2445–2464, https://doi.org/10.1093/petrology/egq063.

Ji, W., Wu, F., Chung, S., and Liu, C., 2014, The Gangdese magmatic constraints on a latest Cretaceous lithospheric delamination of the Lhasa terrane, southern Tibet: Lithos, v. 210–211, p. 168–180, https://doi.org/10.1016/j.lithos.2014.10.001.

Ji, W., Wu, F., Liu, X., Liu, Z., Zhang, C., Liu, T., Wang, J., and Paterson, S.R., 2020, Pervasive Miocene melting of thickened crust from the Lhasa terrane to Himalaya, southern Tibet and its constraint on generation of Himalayan leucogranite: Geochimica et Cosmochimica Acta, v. 278, p. 137–156, https://doi.org/10.1016/j.gca.2019.07.048.

Jolivet, M., Brunel, M., Seward, D., Xu, Z., Yang, J., Roger, F., Tapponnier, P., Malavieille, J., Arnaud, N., and Wu, C., 2001, Mesozoic and Cenozoic tectonics of the northern edge of the Tibetan plateau: Fission-track constraints: Tectonophysics, v. 343, p. 111–134, https://doi.org/10.1016/S0040-1951(01)00196-2.

Kapp, P., and DeCelles, P.G., 2019, Mesozoic-Cenozoic geological evolution of the Himalayan-Tibetan orogen and working tectonic hypotheses: American Journal of Science, v. 319, p. 159–254, https://doi.org/10.2475/03.2019.01.

Kapp, P., DeCelles, P.G., Gehrels, G.E., Heizler, M., and Ding, L., 2007, Geological records of the Lhasa-Qiangtang and Indo-Asian collisions in the Nima area of central Tibet: Geological Society of America Bulletin, v. 119, p. 917–933, https://doi.org/10.1130/B26033.1.

Kesler, S.E., and Wilkinson, B.H., 2006, The role of exhumation in the temporal distribution of ore deposits: Economic Geology, v. 101, p. 919–922, https://doi.org/10.2113/gsecongeo.101.5.919.

Kirby, E., Reiners, P.W., Krol, M.A., Whipple, K.X., Hodges, K.V., Farley, K.A., Tang, W., and Chen, Z., 2002, Late Cenozoic evolution of the eastern margin of the Tibetan Plateau: Inferences from $^{40}Ar/^{39}Ar$ and (U-Th)/He thermochronology: Tectonics, v. 21, https://doi.org/10.1029/2000TC001246.

Laske, G., Masters., G., Ma, Z., and Pasyanos, M., 2013, Update on CRUST1.0—A 1-degree Global Model of Earth's Crust: Geophysical Research Abstracts, v. 15, abstract EGU2013-2658.

Lee, C.A., and Tang, M., 2020, How to make porphyry copper deposits: Earth and Planetary Science Letters, v. 529, https://doi.org/10.1016/j.epsl.2019.115868.

Leng, C., Cooke, D.R., Hou, Z., Evans, N.J., Zhang, X., Chen, W.T., Danišík, M., McInnes, B.I.A., and Yang, J., 2018, Quantifying exhumation at the giant Pulang porphyry Cu-Au deposit using U-Pb-He dating: Economic Geology, v. 113, p. 1077–1092, https://doi.org/10.5382/econgeo.2018.4582.

Li, C., Zhao, Z., Lu, H., and Li, H., 2022, Late Mesozoic-Cenozoic multistage exhumation of the central Bangong-Nujiang Suture, Central Tibet: Tectonophysics, v. 827, https://doi.org/10.1016/j.tecto.2022.229268.

Li, G., Cao, M., Qin, K., Evans, N.J., McInnes, B.I.A., and Liu, Y., 2014, Thermal-tectonic history of the Baogutu porphyry Cu deposit, West Junggar as constrained from zircon U–Pb, biotite Ar/Ar and zircon/apatite (U–Th)/He dating: Journal of Asian Earth Sciences, v. 79, p. 741–758, https://doi.org/10.1016/j.jseaes.2013.05.026.

Li, L., Capitanio, F.A., Cawood, P.A., Wu, B., Zhai, M., and Wang, X., 2024, Double subduction controls on long-lived continental tectonics and subcontinental mantle temperatures: Geology, v. 52, p. 836–840, https://doi.org/10.1130/G52232.1.

Li, S., Wang, Q., Zhu, D., Cawood, P.A., Stern, R.J., Weinberg, R., Zhao, Z., and Mo, X., 2020, Reconciling orogenic drivers for the evolution of the Bangong-Nujiang Tethys during Middle-Late Jurassic: Tectonics, v. 39, https://doi.org/10.1029/2019TC005951.

Li, X., Mo, X., Yu, X., Ding, Y., Huang, X., Wei, P., and He, W., 2013, Geochronological, geochemical and Sr–Nd–Hf isotopic constraints on the origin of the Cretaceous intraplate volcanism in West Qinling, Central China: Implications for asthenosphere–lithosphere interaction: Lithos, v. 177, p. 381–401, https://doi.org/10.1016/j.lithos.2013.05.020.

Li, Z., Gao, J., Zheng, C., Liu, C., Ma, Y., and Zhao, W., 2015, Present-day heat flow and tectonic-thermal evolution since the late Paleozoic time of Qaidam basin: Chinese Journal of Geophysics, v. 58, no. 10, p. 3687–3705 [in Chinese with English abstract].

Liu, K., Li, Z., Shi, X., Wei, X., Ren, Z., Yang, X., and Peng, B., 2020, Late Hercynian-Indosinian denudation and uplift history in the eastern Qaidam Basin: Constraints from multiple thermometric indicators and sedimentary evidences: Chinese Journal of Geophysics, v. 63, no. 4, p. 1403–1421, https://doi.org/10.6038/cjg2020M0566 [in Chinese with English abstract].

Liu, S., Xu, X., Nocquet, J., Chen, G., Tan, X., Jónsson, S., and Klinger, Y., 2025, Lower crustal thickening drives active uplift in Northern Tibet: Earth and Planetary Science Letters, v. 655, https://doi.org/10.1016/j.epsl.2025.119245.

Liu, Y., et al., 2022, Jurassic tectonic evolution of Tibetan Plateau: A review of Bangong-Nujiang Meso-Tethys Ocean: Earth-Science Reviews, v. 227, https://doi.org/10.1016/j.earscirev.2022.103973.

Ma, L., Wang, Q., Li, Z., Wyman, D.A., Jiang, Z., Yang, J., Gou, G., and Guo, H., 2013a, Early Late Cretaceous (ca. 93 Ma) norites and hornblendites in the Milin area, eastern Gangdese: Lithosphere–asthenosphere interaction during slab roll-back and an insight into early Late Cretaceous (ca. 100–80 Ma) magmatic "flare-up" in southern Lhasa (Tibet): Lithos, v. 172–173, p. 17–30, https://doi.org/10.1016/j.lithos.2013.03.007.

Ma, L., Wang, Q., Wyman, D.A., Li, Z., Jiang, Z., Yang, J., Gou, G., and Guo, H., 2013b, Late Cretaceous (100–89 Ma) magnesian charnockites with adakitic affinities in the Milin area, eastern Gangdese: Partial melting of subducted oceanic crust and implications for crustal growth in southern Tibet: Lithos, v. 175–176, p. 315–332, https://doi.org/10.1016/j.lithos.2013.04.006.

Ma, L., Kerr, A.C., Wang, Q., Jiang, Z., and Hu, W., 2018, Early Cretaceous (~140 Ma) aluminous A-type granites in the Tethyan Himalaya, Tibet: Products of crust-mantle interaction during lithospheric extension: Lithos, v. 300–301, p. 212–226, https://doi.org/10.1016/j.lithos.2017.11.023.

Ma, L., Wang, Q., Kerr, A.C., and Tang, G., 2021, Nature of the pre-collisional lithospheric mantle in Central Tibet: Insights to Tibetan Plateau uplift: Lithos, v. 388–389, https://doi.org/10.1016/j.lithos.2021.106076.

Manea, V.C., Pérez-Gussinyé, M., and Manea, M., 2012, Chilean flat slab subduction controlled by overriding plate thickness and trench rollback: Geology, v. 40, p. 35–38, https://doi.org/10.1130/G32543.1.

Mao, J., Luo, M., Xie, G., Liu, J., and Wu, S., 2014, Basic characteristics and new advances in research and exploration on porphyry copper deposits: Acta Geologica Sinica, v. 88, no. 12, p. 2153–2175 [in Chinese with English abstract].

McRivette, M.W., Yin, A., Chen, X., and Gehrels, G.E., 2019, Cenozoic basin evolution of the central Tibetan plateau as constrained by U-Pb detrital zircon geochronology, sandstone petrology, and fission-track thermochronology: Tectonophysics, v. 751, p. 150–179, https://doi.org/10.1016/j.tecto.2018.12.015.

Min, K., and Gao, J., 2022, Application of low-temperature thermochronology on ore deposits preservation framework in South China: A review: Acta Geochimica, v. 41, p. 165–184, https://doi.org/10.1007/s11631-021-00506-x.

Molnar, P., England, P., and Martinod, J., 1993, Mantle dynamics, uplift of the Tibetan Plateau, and the Indian Monsoon: Reviews of Geophysics, v. 31, p. 357–396, https://doi.org/10.1029/93RG02030.

Mulch, A., and Chamberlain, C.P., 2006, The rise and growth of Tibet: Nature, v. 439, p. 670–671, https://doi.org/10.1038/439670a.

Ouimet, W., Whipple, K., Royden, L., Reiners, P., Hodges, K., and Pringle, M., 2010, Regional incision of the eastern margin of the Tibetan Plateau: Lithosphere, v. 2, p. 50–63, https://doi.org/10.1130/L57.1.

Park, J., Campbell, I.H., Kim, J., and Moon, J., 2015, The role of late sulfide saturation in the formation of a Cu- and Au-rich magma: Insights from the platinum group element geochemistry of Niuatahi–Motutahi lavas, Tonga rear arc: Journal of Petrology, v. 56, p. 59–81, https://doi.org/10.1093/petrology/egu071.

Park, J., Campbell, I.H., Malaviarachchi, S.P.K., Cocker, H., Hao, H., and Kay, S.M., 2019, Chalcophile element fertility and the formation of porphyry Cu ± Au deposits: Mineralium Deposita, v. 54, p. 657–670, https://doi.org/10.1007/s00126-018-0834-0.

Park, J., Campbell, I.H., Chiaradia, M., Hao, H., and Lee, C., 2021, Crustal magmatic controls on the formation of porphyry copper deposits: Nature Reviews: Earth & Environment, v. 2, p. 542–557, https://doi.org/10.1038/s43017-021-00182-8.

Qi, B., Hu, D., Yang, X., Zhang, Y., Tan, C., Zhang, P., and Feng, C., 2016, Apatite fission track study of the Cretaceous-Cenozoic stepwise uplift of the middle segment of the Qilian Mountain: Acta Geoscientica Sinica, v. 37, no. 1, p. 46–58, https://doi.org/10.3975/cagsb.2016.01.05 [in Chinese with English abstract].

Qi, Y., Wang, Q., Zhu, Y., Shi, L., and Yang, Y., 2020, Miocene olivine leucitites in the Hoh Xil Basin, northern Tibet: Implications for intracontinental lithosphere melting and surface uplift of the Tibetan Plateau: Journal of Petrology, v. 61, https://doi.org/10.1093/petrology/egaa026.

Ratschbacher, L., Hacker, B.R., Calvert, A., Webb, L.E., Grimmer, J.C., McWilliams, M.O., Ireland, T., Dong, S., and Hu, J., 2003, Tectonics of the Qinling (Central China): Tectonostratigraphy, geochronology, and deformation history: Tectonophysics, v. 366, p. 1–53, https://doi.org/10.1016/S0040-1951(03)00053-2.

Reid, A., Wilson, C.J.L., Shun, L., Pearson, N., and Belousova, E., 2007, Mesozoic plutons of the Yidun Arc, SW China: U/Pb geochronology and Hf isotopic signature: Ore Geology Reviews, v. 31, p. 88–106, https://doi.org/10.1016/j.oregeorev.2004.11.003.

Reiners, P.W., 2007, Thermochronologic approaches to paleotopography: Reviews in Mineralogy and Geochemistry, v. 66, p. 243–267, https://doi.org/10.2138/rmg.2007.66.10.

Reiners, P.W., and Brandon, M.T., 2006, Using thermochronology to understand orogenic erosion: Annual Review of Earth and Planetary Sciences, v. 34, p. 419–466, https://doi.org/10.1146/annurev.earth.34.031405.125202.

Richards, J.P., 2003, Tectono-magmatic precursors for porphyry Cu-(Mo-Au): Deposit formation: Economic Geology, v. 98, p. 1515–1533, https://doi.org/10.2113/gsecongeo.98.8.1515.

Richards, J.P., 2009, Postsubduction porphyry Cu-Au and epithermal Au deposits: Products of remelting of subduction-modified lithosphere: Geology, v. 37, p. 247–250, https://doi.org/10.1130/G25451A.1.

Richards, J.P., 2015, The oxidation state, and sulfur and Cu contents of arc magmas: Implications for metallogeny: Lithos, v. 233, p. 27–45, https://doi.org/10.1016/j.lithos.2014.12.011.

Richards, J.P., 2022, Porphyry copper deposit formation in arcs: What are the odds?: Geosphere, v. 18, p. 130–155, https://doi.org/10.1130/GES02086.1.

Roger, F., Jolivet, M., and Malavieille, J., 2010, The tectonic evolution of the Songpan-Garzê (North Tibet) and adjacent areas from Proterozoic to Present: A synthesis: Journal of Asian Earth Sciences, v. 39, p. 254–269, https://doi.org/10.1016/j.jseaes.2010.03.008.

Rohrmann, A., Kapp, P., Carrapa, B., Reiners, P.W., Guynn, J., Ding, L., and Heizler, M., 2012, Thermochronologic evidence for plateau formation in central Tibet by 45 Ma: Geology, v. 40, p. 187–190, https://doi.org/10.1130/G32530.1.

Rowley, D.B., and Currie, B.S., 2006, Palaeo-altimetry of the late Eocene to Miocene Lunpola basin, central Tibet: Nature, v. 439, p. 677–681, https://doi.org/10.1038/nature04506.

Royden, L.H., Burchfiel, B.C., King, R.W., Wang, E., Chen, Z., Shen, F., and Liu, Y., 1997, Surface deformation and lower crustal flow in eastern Tibet: Science, v. 276, p. 788–790, https://doi.org/10.1126/science.276.5313.788.

Royden, L.H., Burchfiel, B.C., and van der Hilst, R.D., 2008, The geological evolution of the Tibetan Plateau: Science, v. 321, p. 1054–1058, https://doi.org/10.1126/science.1155371.

Sillitoe, R.H., 1972, A plate tectonic model for the origin of porphyry copper deposits: Economic Geology, v. 67, p. 184–197, https://doi.org/10.2113/gsecongeo.67.2.184.

Sillitoe, R.H., 2010, Porphyry copper systems: Economic Geology, v. 105, p. 3–41, https://doi.org/10.2113/gsecongeo.105.1.3.

Singer, D.A., Berger, V.I., and Moring, B.C., 2008, Porphyry copper deposits of the world: Database, map, and grade and tonnage models: U.S. Geological Survey Open-File Report 2008-1155, 45 p., https://doi.org/10.3133/ofr20081155.

Spicer, R.A., Harris, N.B.W., Widdowson, M., Herman, A.B., Guo, S., Valdes, P.J., Wolfe, J.A., and Kelley, S.P., 2003, Constant elevation of southern Tibet over the past 15 million years: Nature, v. 421, p. 622–624, https://doi.org/10.1038/nature01356.

Spicer, R.A., Su, T., Valdes, P.J., Farnsworth, A., Wu, F., Shi, G., Spicer, T.E.V., and Zhou, Z., 2021, Why 'the uplift of the Tibetan Plateau' is a myth: National Science Review, v. 8, https://doi.org/10.1093/nsr/nwaa091.

Staisch, L.M., Niemi, N.A., Hong, C., Clark, M.K., Rowley, D.B., and Currie, B., 2014, A Cretaceous-Eocene depositional age for the Fenghuoshan Group, Hoh Xil Basin: Implications for the tectonic evolution of the northern Tibet Plateau: Tectonics, v. 33, p. 281–301, https://doi.org/10.1002/2013TC003367.

Staisch, L.M., Niemi, N.A., Clark, M.K., and Chang, H., 2016, Eocene to late Oligocene history of crustal shortening within the Hoh Xil Basin and implications for the uplift history of the northern Tibetan Plateau: Tectonics, v. 35, p. 862–895, https://doi.org/10.1002/2015TC003972.

Su, T., et al., 2019a, Uplift, climate and biotic changes at the Eocene–Oligocene transition in south-eastern Tibet: National Science Review, v. 6, p. 495–504, https://doi.org/10.1093/nsr/nwy062.

Su, T., et al., 2019b, No high Tibetan Plateau until the Neogene: Science Advances, v. 5, https://doi.org/10.1126/sciadv.aav2189.

Su, T., et al., 2020, A Middle Eocene lowland humid subtropical "Shangri-La" ecosystem in central Tibet: Proceedings of the National Academy of Sciences of the United States of America, v. 117, p. 32,989–32,995, https://doi.org/10.1073/pnas.2012647117.

Su, W., He, Z., Zhong, L., Glorie, S., Zhong, K., Jepson, G., and De Grave, J., 2022, Late Oligocene–Miocene morpho-tectonic evolution of the central Gangdese batholith constrained by low-temperature thermochronology: Tectonophysics, v. 840, https://doi.org/10.1016/j.tecto.2022.229559.

Tan, X., Lee, Y., Xu, X., and Cook, K.L., 2017, Cenozoic exhumation of the Danba antiform, eastern Tibet: Evidence from low-temperature thermochronology: Lithosphere, v. 9, p. 534–544, https://doi.org/10.1130/L613.1.

Tang, J., 2019, Mineral resources base investigation and research status of the Tibet Plateau and its adjacent major metallogenic belts: Acta Petrologica Sinica (Yanshi Xuebao), v. 35, p. 617–624 [in Chinese with English abstract].

Tang, J., Lin, B., Yang, H., Tang, P., Xie, F., Wang, Y., Zhou, A., Gu, F., Zou, B., Zhang, X., Wang, Q., Li, F., Zhang, Q., Fu, X., Zhang, R., Yu, L., Wang, M., Xiong, Y., Xie, J., and Li, W., 2024, Geological characteristics and prospecting direction of porphyry-skarn-epithermal deposits in Xizang: Mineralium Deposita, v. 43, no. 6, p. 1223–1265 [in Chinese with English abstract].

Tapponnier, P., Peltzer, G., Le Dain, A.Y., Armijo, R., and Cobbold, P., 1982, Propagating extrusion tectonics in Asia: New insights from simple experiments with plasticine: Geology, v. 10, p. 611–616, https://doi.org/10.1130/0091-7613(1982)10<611:PETIAN>2.0.CO;2.

Tapponnier, P., Zhiqin, X., Roger, F., Meyer, B., Arnaud, N., Wittlinger, G., and Jingsui, Y., 2001, Oblique stepwise rise and growth of the Tibet Plateau: Science, v. 294, p. 1671–1677, https://doi.org/10.1126/science.105978.

Tian, Y., Kohn, B.P., Gleadow, A.J.W., and Hu, S., 2014, A thermochronological perspective on the morphotectonic evolution of the southeastern Tibetan Plateau: Journal of Geophysical Research: Solid Earth, v. 119, p. 676–698, https://doi.org/10.1002/2013JB010429.

Turner, S., Arnaud, N., Liu, J., Rogers, N., Hawkesworth, C., Harris, N., Kelley, S., Van Calsteren, P., and Deng, W., 1996, Post-collision, shoshonitic volcanism on the Tibetan Plateau: Implications for convective thinning of the lithosphere and the source of ocean island basalts: Journal of Petrology, v. 37, p. 45–71, https://doi.org/10.1093/petrology/37.1.45.

van der Beek, P., and Schildgen, T.F., 2023, Short communication: age2exhume—A MATLAB/Python script to calculate steady-state vertical exhumation rates from thermochronometric ages and application to the Himalaya: Geochronology, v. 5, p. 35–49, https://doi.org/10.5194/gchron-5-35-2023.

Vincent, S.J., and Allen, M.B., 1999, Evolution of the Minle and Chaoshui Basins, China: Implications for Mesozoic strike-slip basin formation in Central Asia: Geological Society of America Bulletin, v. 111, p. 725–742, https://doi.org/10.1130/0016-7606(1999)111<0725:EOTMAC>2.3.CO;2.

Wan, B., Wu, F., Chen, L., Zhao, L., Liang, X., Xiao, W., and Zhu, R., 2019, Cyclical one-way continental rupture-drift in the Tethyan evolution: Subduction-driven plate tectonics: Science China Earth Sciences, v. 62, p. 2005–2016, https://doi.org/10.1007/s11430-019-9393-4.

Wang, C., Zhao, X., Liu, Z., Lippert, P.C., Graham, S.A., Coe, R.S., Yi, H., Zhu, L., Liu, S., and Li, Y., 2008a, Constraints on the early uplift history of the Tibetan Plateau: Proceedings of the National Academy of Sciences of the United States of America, v. 105, p. 4987–4992, https://doi.org/10.1073/pnas.0703595105.

Wang, C., Dai, J., Zhao, X., Li, Y., Graham, S.A., He, D., Ran, B., and Meng, J., 2014, Outward-growth of the Tibetan Plateau during the Cenozoic: A review: Tectonophysics, v. 621, p. 1–43, https://doi.org/10.1016/j.tecto.2014.01.036.

Wang, S., Fan, C., Wang, G., and Wang, E., 2008b, Late Cenozoic deformation along the northwestern continuation of the Xianshuihe fault system, Eastern Tibetan Plateau: Geological Society of America Bulletin, v. 120, p. 312–327, https://doi.org/10.1130/B25833.1.

Wang, X., Song, C., Zattin, M., He, P., Song, A., Li, J., and Wang, Q., 2016, Cenozoic pulsed deformation history of northeastern Tibetan Plateau reconstructed from fission-track thermochronology: Tectonophysics, v. 672–673, p. 212–227, https://doi.org/10.1016/j.tecto.2016.02.006.

Wilkinson, B.H., and Kesler, S.E., 2007, Tectonism and exhumation in convergent margin orogens: Insights from ore deposits: The Journal of Geology, v. 115, p. 611–627, https://doi.org/10.1086/521606.

Wilkinson, J.J., 2013, Triggers for the formation of porphyry ore deposits in magmatic arcs: Nature Geoscience, v. 6, p. 917–925, https://doi.org/10.1038/ngeo1940.

Willett, S.D., 1999, Orogeny and orography: The effects of erosion on the structure of mountain belts: Journal of Geophysical Research: Solid Earth, v. 104, p. 28,957–28,981, https://doi.org/10.1029/1999JB900248.

Wilson, C.J.L., and Fowler, A.P., 2011, Denudational response to surface uplift in east Tibet: Evidence from apatite fission-track thermochronology: Geological Society of America Bulletin, v. 123, p. 1966–1987, https://doi.org/10.1130/B30331.1.

Wilson, C.J.L., Harrowfield, M.J., and Reid, A.J., 2006, Brittle modification of Triassic architecture in eastern Tibet: Implications for the construction of the Cenozoic plateau: Journal of Asian Earth Sciences, v. 27, p. 341–357, https://doi.org/10.1016/j.jseaes.2005.04.004.

Xia, R., Wang, C., Deng, J., Carranza, E.J.M., Li, W., and Qing, M., 2014a, Crustal thickening prior to 220 Ma in the East Kunlun Orogenic Belt: Insights from the Late Triassic granitoids in the Xiao-Nuomuhong pluton: Journal of Asian Earth Sciences, v. 93, p. 193–210, https://doi.org/10.1016/j.jseaes.2014.07.013.

Xia, Y., Zhu, D., Wang, Q., Zhao, Z., Liu, D., Wang, L., and Mo, X., 2014b, Picritic porphyrites and associated basalts from the remnant Comei Large Igneous Province in SE Tibet: Records of mantle-plume activity: Terra Nova, v. 26, p. 487–494, https://doi.org/10.1111/ter.12124.

Xiong, Z., et al., 2020, The early Eocene rise of the Gonjo Basin, SE Tibet: From low desert to high forest: Earth and Planetary Science Letters, v. 543, https://doi.org/10.1016/j.epsl.2020.116312.

Xu, G., and Kamp, P.J.J., 2000, Tectonics and denudation adjacent to the Xianshuihe Fault, eastern Tibetan Plateau: Constraints from fission track thermochronology: Journal of Geophysical Research: Solid Earth, v. 105, p. 19,231–19,251, https://doi.org/10.1029/2000JB900159.

Xu, Q., Li, S., and Bai, Y., 2022, Modern-like elevation and climate in Tibet since the mid-Miocene (ca. 15 Ma): Geological Society of America Bulletin, v. 134, p. 2561–2575, https://doi.org/10.1130/B36198.1.

Yang, H., Song, Y., Tang, J., Wang, Q., Gao, K., and Wei, S., 2020, Low temperature history of the Tiegelongnan porphyry–epithermal Cu (Au) deposit in the Duolong ore district of northwest Tibet, China: Resource Geology, v. 70, p. 111–124, https://doi.org/10.1111/rge.12221.

Yang, H., Fang, X., Song, Y., Lin, B., Li, Y., Wang, Q., Liu, Z., He, L., Zhang, Q., and Fu, X., 2022a, Thermal history of the Naruo porphyry deposit in the Duolong ore district, western Tibet: Evidence from U-Pb, $^{40}Ar/^{39}Ar$ and (U-Th)/He thermochronology: Acta Geologica Sinica (English Edition), v. 96, p. 2015–2027, https://doi.org/10.1111/1755-6724.14955.

Yang, H., Tang, J., Song, Y., Wang, Q., and Liu, Z., 2022b, The preservation mechanism of the Duolong ore district in northwest Tibet: Evidence from the low temperature thermochronological study: Ore Geology Reviews, v. 143, https://doi.org/10.1016/j.oregeorev.2022.104766.

Yang, Z., and Cao, K., 2024, Post-collisional porphyry copper deposits in Tibet: An overview: Earth-Science Reviews, v. 258, https://doi.org/10.1016/j.earscirev.2024.104954.

Yanites, B.J., and Kesler, S.E., 2015, A climate signal in exhumation patterns revealed by porphyry copper deposits: Nature Geoscience, v. 8, p. 462–465, https://doi.org/10.1038/ngeo2429.

Ye, Z., Gao, R., Li, Q., Zhang, H., Shen, X., Liu, X., and Gong, C., 2015, Seismic evidence for the North China plate underthrusting beneath northeastern Tibet and its implications for plateau growth: Earth and Planetary Science Letters, v. 426, p. 109–117, https://doi.org/10.1016/j.epsl.2015.06.024.

Yin, A., and Harrison, T.M., 2000, Geologic evolution of the Himalayan-Tibetan orogen: Annual Review of Earth and Planetary Sciences, v. 28, p. 211–280, https://doi.org/10.1146/annurev.earth.28.1.211.

Yin, J., Wang, Y., Hodges, K.V., Xiao, W., Thomson, S.N., Chen, W., Yuan, C., Sun, M., Cai, K., and Sun, J., 2023, Episodic long-term exhumation of the Tianshan Orogenic Belt: New insights from multiple low-temperature thermochronometers: Tectonics, v. 42, https://doi.org/10.1029/2022TC007469.

Zhang, B., Liu, J., Chen, W., Zhang, Z., Yang, L., Zhang, L., Zhu, Z., Sun, C., and Sun, Z., 2024a, Ongoing India–Asia convergence controlled differential growth of the eastern Tibetan Plateau: Gondwana Research, v. 126, p. 386–405, https://doi.org/10.1016/j.gr.2023.11.001.

Zhang, J., Wang, Y., Zhang, B., and Zhao, H., 2015, Evolution of the NE Qinghai–Tibetan Plateau, constrained by the apatite fission track ages of the mountain ranges around the Xining Basin in NW China: Journal of Asian Earth Sciences, v. 97, p. 10–23, https://doi.org/10.1016/j.jseaes.2014.10.002.

Zhang, J., Sinclair, H.D., Li, Y., Wang, C., Persano, C., Qian, X., Han, Z., Yao, X., and Duan, Y., 2019, Subsidence and exhumation of the Mesozoic Qiangtang Basin: Implications for the growth of the Tibetan plateau: Basin Research, v. 31, p. 754–781, https://doi.org/10.1111/bre.12343.

Zhang, P., Wang, G., Feng, Y., Wang, Y., Wang, H., He, C., Yan, P., and Chen, Z., 2024b, Exhumation and preservation of the Bangbule Pb-Zn-Cu deposit in the western Gangdese Metallogenic Belt, Tibet: Constraints from fission track thermochronology and fault gouge dating: Ore Geology Reviews, v. 167, https://doi.org/10.1016/j.oregeorev.2024.105993.

Zhang, X., et al., 2022, Rapid Eocene diversification of spiny plants in subtropical woodlands of central Tibet: Nature Communications, v. 13, 3787, https://doi.org/10.1038/s41467-022-31512-z.

Zhang, Z., Kusky, T., Gao, M., and Cheng, Q., 2023, Spatiotemporal analysis of big data sets of detrital zircon U-Pb geochronology and Hf isotope data: Tests of tectonic models for the Precambrian evolution of the North China Craton: Earth-Science Reviews, v. 239, https://doi.org/10.1016/j.earscirev.2023.104372.

Zhao, J., Qin, K., Xiao, B., McInnes, B., Li, G., Evans, N., Cao, M., and Li, J., 2016, Thermal history of the giant Qulong Cu–Mo deposit, Gangdese metallogenic belt, Tibet: Constraints on magmatic–hydrothermal evolution and exhumation: Gondwana Research, v. 36, p. 390–409, https://doi.org/10.1016/j.gr.2015.07.005.

Zhao, Z., Li, C., Ma, X., and Li, H., 2022a, A compilation of new and existing thermochronology data concerning the Lhasa terrane combined with a geological synthesis of the area: Acta Geologica Sinica (English Edition), v. 96, p. 1534–1544, https://doi.org/10.1111/1755-6724.14806.

Zhao, Z., Lu, H., Wang, S., Li, H., Li, C., Liu, D., Pan, J., Zheng, Y., and Bai, M., 2022b, The Cenozoic multiple-stage uplift of the Qiangtang Terrane, Tibetan Plateau: Frontiers of Earth Science, v. 10, https://doi.org/10.3389/feart.2022.818079.

Zhao, Z.B., Bons, P.D., Li, C., Wang, G.H., Ma, X.X., and Li, G.W., 2020, The Cretaceous crustal shortening and thickening of the South Qiangtang Terrane and implications for proto-Tibetan Plateau formation: Gondwana Research, v. 78, p. 141–155, https://doi.org/10.1016/j.gr.2019.09.003.

Zhu, D., Mo, X., Pan, G., Zhao, Z., Dong, G., Shi, Y., Liao, Z., Wang, L., and Zhou, C., 2008, Petrogenesis of the earliest Early Cretaceous mafic rocks from the Cona area of the eastern Tethyan Himalaya in south Tibet: Interaction between the incubating Kerguelen plume and the eastern Greater India lithosphere?: Lithos, v. 100, p. 147–173, https://doi.org/10.1016/j.lithos.2007.06.024.

Zhu, D., Chung, S., Mo, X., Zhao, Z., Niu, Y., Song, B., and Yang, Y., 2009, The 132 Ma Comei-Bunbury large igneous province: Remnants identified in present-day southeastern Tibet and southwestern Australia: Geology, v. 37, p. 583–586, https://doi.org/10.1130/G30001A.1.

Zhu, D., Wang, Q., Zhao, Z., Chung, S., Cawood, P.A., Niu, Y., Liu, S., Wu, F., and Mo, X., 2015, Magmatic record of India-Asia collision: Scientific Reports, v. 5, https://doi.org/10.1038/srep14289.

Zhu, D., Li, S., Cawood, P.A., Wang, Q., Zhao, Z., Liu, S., and Wang, L., 2016, Assembly of the Lhasa and Qiangtang terranes in central Tibet by divergent double subduction: Lithos, v. 245, p. 7–17, https://doi.org/10.1016/j.lithos.2015.06.023.

Zhu, D., Wang, Q., Cawood, P.A., Zhao, Z., and Mo, X., 2017, Raising the Gangdese Mountains in southern Tibet: Journal of Geophysical Research: Solid Earth, v. 122, p. 214–223, https://doi.org/10.1002/2016JB013508.

Science Editor: Wenjiao Xiao
Associate Editor: Timothy Kusky

Manuscript Received 22 May 2025
Revised Manuscript Received 5 December 2025
Manuscript Accepted 29 January 2026